



<b>Publication Year</b>	2017
<b>Acceptance in OA</b>	2020-09-01T13:17:47Z
<b>Title</b>	FRICAT: A FIRST catalog of FRI radio galaxies
<b>Authors</b>	CAPETTI, Alessandro, MASSARO, Francesco, BALDI, RANIERI DIEGO
<b>Publisher's version (DOI)</b>	10.1051/0004-6361/201629287
<b>Handle</b>	<a href="http://hdl.handle.net/20.500.12386/27032">http://hdl.handle.net/20.500.12386/27032</a>
<b>Journal</b>	ASTRONOMY & ASTROPHYSICS
<b>Volume</b>	598

# FRICAT: A FIRST catalog of FR I radio galaxies

A. Capetti<sup>1</sup>, F. Massaro<sup>2</sup>, and R. D. Baldi<sup>3</sup>

<sup>1</sup> INAF–Osservatorio Astrofisico di Torino, via Osservatorio 20, 10025 Pino Torinese, Italy  
e-mail: capetti@oato.inaf.it

<sup>2</sup> Dipartimento di Fisica, Università degli Studi di Torino, via Pietro Giuria 1, 10125 Torino, Italy

<sup>3</sup> Department of Physics and Astronomy, University of Southampton, Highfield, SO17 1BJ, UK

Received 11 July 2016 / Accepted 30 September 2016

## ABSTRACT

We built a catalog of 219 FR I radio galaxies (FR Is), called FRICAT, selected from a published sample and obtained by combining observations from the NVSS, FIRST, and SDSS surveys. We included in the catalog the sources with an edge-darkened radio morphology, redshift  $\leq 0.15$ , and extending (at the sensitivity of the FIRST images) to a radius  $r$  larger than 30 kpc from the center of the host. We also selected an additional sample (sFRICAT) of 14 smaller ( $10 < r < 30$  kpc) FR Is, limiting to  $z < 0.05$ . The hosts of the FRICAT sources are all luminous ( $-21 \geq M_r \geq -24$ ), red early-type galaxies with black hole masses in the range  $10^8 \lesssim M_{\text{BH}} \lesssim 3 \times 10^9 M_{\odot}$ ; the spectroscopic classification based on the optical emission line ratios indicates that they are all low excitation galaxies. Sources in the FRICAT are then indistinguishable from the FR Is belonging to the Third Cambridge Catalogue of Radio Sources (3C) on the basis of their optical properties. Conversely, while the 3C-FR Is show a strong positive trend between radio and [O III] emission line luminosity, these two quantities are unrelated in the FRICAT sources; at a given line luminosity, they show radio luminosities spanning about two orders of magnitude and extending to much lower ratios between radio and line power than 3C-FR Is. Our main conclusion is that the 3C-FR Is just represent the tip of the iceberg of a much larger and diverse population of FR Is.

**Key words.** galaxies: active – galaxies: jets

## 1. Introduction

Fanaroff & Riley (1974) introduced the first classification scheme for extragalactic radio sources with large-scale structures (i.e., greater than  $\sim 15$ – $20$  kpc in size). They proposed to distinguish radio sources into two main classes on the basis of the relation between relative positions of regions of high and low surface brightness in their extended components. This scheme was based on the ratio  $R_{\text{FR}}$  of the distance between the regions of highest surface brightness on opposite sides of the central host galaxy to the total extent of the source up to the lowest brightness contour in the radio images. Radio sources with  $R_{\text{FR}} < 0.5$  were placed in Class I (i.e., the edge-darkened FR Is) and sources with  $R_{\text{FR}} > 0.5$  in Class II (i.e., the edge-brightened FR IIs).

This morphology-based classification scheme was also linked to their intrinsic power, when Fanaroff and Riley found that all sources in their sample with luminosity at 178 MHz smaller than  $2 \times 10^{25} \text{ W Hz}^{-1} \text{ sr}^{-1}$  (for a Hubble constant of  $50 \text{ km s}^{-1} \text{ Mpc}^{-1}$ ) were classified as FR I while the brighter sources all were FR II. The luminosity distinction between FR classes is fairly sharp at 178 MHz but their separation is cleaner in the optical-radio luminosity plane, implying that the FR I/FR II dichotomy depends on optical and radio luminosity (Ledlow & Owen 1996).

The selection of large and well-defined samples of radio galaxies is of great importance to properly address several issues, such as building their luminosity functions, exploring the properties of their hosts, studying their environment and their cosmic evolution, and comparing the results obtained for the different

classes of radio-galaxies for radio-quiet active nuclei and for the population of quiescent galaxies.

In particular, the number of known FR I radio galaxies is rather small. For example the Third Cambridge Catalogue of Radio Sources (3C; Bennett 1962) includes less than  $\sim 30$  FR Is. The second Bologna sample (B2; Colla et al. 1975; Fanti et al. 1978) is formed by  $\sim 100$  radio galaxies of lower luminosity than those of the 3C; most of these have a luminosity below the FR I/FR II transition and about half of them are FR I. These samples are not sufficiently large to address the issues listed above properly. Furthermore, as these samples are selected with a rather high flux threshold, they present a limited (and possibly statistically biased) view of the FR I population.

The advent of large area surveys opens the opportunity to set the results on several key issues on strong statistical foundations. In particular, the radio, infrared, and optical observations available thanks to recent large-area surveys are a unique tool in the analysis of the radio galaxies and quasars, since they allow us to identify large numbers of radio sources, obtain spectroscopic redshifts, and determine the properties of their hosts. Best et al. (2005), Baldi & Capetti (2010), and Best & Heckman (2012) already used the extensive multifrequency information available to analyze the properties of the population of low redshift radio emitting AGN. We here also consider the radio morphological information and explore the possibility to create the first catalog of FR I radio galaxies selected on the basis of radio and optical data, which we call the FRICAT.

This paper is organized as follows. In Sect. 2 we present the selection criteria of the sample of FR Is, whose completeness

is discussed in Sect. 3. The radio and optical properties of the selected sources are presented in Sect. 4 and discussed in Sect. 5. Section 6 is devoted to our summary and conclusions.

Throughout the paper we adopt a cosmology with  $H_0 = 67.8 \text{ km s}^{-1} \text{ Mpc}^{-1}$ ,  $\Omega_M = 0.308$ , and  $\Omega_\Lambda = 0.692$  (Planck Collaboration XIII 2016).

For our numerical results, we use c.g.s. units unless stated otherwise. Spectral indices  $\alpha$  are defined by the usual convention on the flux density,  $S_\nu \propto \nu^{-\alpha}$ . The SDSS magnitudes are in the AB system and are corrected for the Galactic extinction; WISE magnitudes are instead in the Vega system and are not corrected for extinction since, as shown by, for example, D’Abrusco et al. (2014), such correction affects only the magnitude at  $3.4 \mu$  of sources lying at low Galactic latitudes (and by less than  $\sim 3\%$ ).

## 2. Sample selection

We searched for FR I radio galaxies in the sample of 18 286 radio sources built by Best & Heckman (Best & Heckman 2012, hereafter the BH12 sample) by limiting our search to the subsample of objects in which, according to these authors, the radio emission is produced by an active nucleus. They cross-matched the optical spectroscopic catalogs produced by the group from the Max Planck Institute for Astrophysics and The Johns Hopkins University (Brinchmann et al. 2004; Tremonti et al. 2004) based on data from the data release 7 of the Sloan Digital Sky Survey (DR7/SDSS; Abazajian et al. 2009)<sup>1</sup>, with the National Radio Astronomy Observatory Very Large Array Sky Survey (NVSS; Condon et al. 1998) and the Faint Images of the Radio Sky at Twenty centimeters survey (FIRST; Becker et al. 1995) adopting a radio flux density limit of 5 mJy in the NVSS. We focused on the 3,357 sources with redshift  $z < 0.15$ .

We visually inspected all the FIRST images of each individual source and preserved only those whose radio emission reaches a distance of at least 30 kpc from the center of the optical host at the sensitivity of the FIRST images. Such a radius corresponds to  $11''4$  for the farthest objects; this ensures that all the 741 selected sources are well resolved with the  $5''$  resolution of the FIRST images. This permitted us to properly explore their morphology. The reference surface brightness level adopted is 0.45 mJy/beam (approximately three times the typical rms of the FIRST images) for the objects at  $z = 0.15$ . The brightness level is increased by a factor  $[(1+0.15)/(1+z)]^4$  for closer objects to compensate for the cosmological surface brightness dimming; this level corresponds to a correction factor of  $\sim 1.75$  for  $z = 0$ . We also applied a  $k$  correction by assuming a spectral index of 0.7, which is typical of the extended radio emission; in this case the correction is rather small, amounting to at most  $\sim 10\%$ .

We adopted a purely morphological classification based on the radio structure shown by the FIRST images. The original FR I definition corresponds to “a great diversity of structure” (Fanaroff & Riley 1974), and it is not always of easy application. We adopted rather strict criteria for a positive classification for the selection of the FIRST sample of FR Is. We limited our selection to the sources showing one-sided or two-sided jets in which the surface brightness is generally decreasing along its whole length, lacking of any brightness enhancement at the jet end. We allowed for bent jets and we thus included narrow angle tail (NAT; Rudnick & Owen 1977) sources; conversely, we excluded the sources in which a substantial brightening occurs along the jet, thus excluding, for example, wide angle tail (WAT; Owen & Rudnick 1976) objects.

<sup>1</sup> Available at <http://www.mpa-garching.mpg.de/SDSS/>.

The three authors performed this analysis independently and we included only the sources for which a FR I classification is proposed by at least two of us.

The resulting sample, to which we refer as FRICAT, is formed by 219 FR Is. In Fig. 1 we present the FIRST images of the first 12 FRICAT sources selected to illustrate the outcome of our selection. Images of all FRICAT objects are available in the Appendix. Their main properties are presented in Table B.1, where we report the SDSS name, redshift, and NVSS 1.4 GHz flux density (from BH12). The [O III] line flux, the  $r$ -band SDSS AB magnitude,  $m_r$ , the Dn(4000) index (see Sect. 4 for the definition of the Dn(4000)), and the stellar velocity dispersion  $\sigma_*$  are instead from the MPA-JHU DR7 release of spectrum measurements. The concentration index  $C_r$  was obtained for each source directly from the SDSS database. For sake of clarity, errors are not shown in the table; we estimated a median error of 0.08 on  $C_r$ , of 0.03 on Dn(4000), of 0.004 magnitudes on  $m_r$ , and of  $9 \text{ km s}^{-1}$  on  $\sigma_*$ . Finally we list the resulting radio and line luminosity, and the black hole masses estimated from the stellar velocity dispersion and the relation  $\sigma_* - M_{\text{BH}}$  of Tremaine et al. (2002). The error in the  $M_{\text{BH}}$  is dominated by the spread of the relation used (rather than by the errors in the measurements of  $\sigma_*$ ) resulting in an uncertainty of a factor  $\sim 2$ .

The limited resolution of FIRST imposes a minimum size of 30 kpc to the FR Is. We selected (with the same criteria discussed above) a second sample of FR Is extending to smaller radii,  $10 < r < 30 \text{ kpc}$ , to consider also less extended radio sources. We limited this sample to nearby objects ( $z < 0.05$ ) to preserve a sufficient spatial resolution. The images of these 14 sources, forming the “small” FR Is sample (hereafter sFRICAT), are presented in Fig. 2 and their properties are listed in Table B.2.

## 3. The completeness of the FRICAT samples

We now discuss the completeness of the sample related to the radio and optical selection.

Concerning the radio selection, the BH12 includes sources with a NVSS flux density larger than 5 mJy. However, our selection also depends on the brightness distribution in the FIRST images. Therefore we might be missing objects characterized by, for example, diffuse emission not reaching the  $3\sigma$  limit in these higher resolution images; furthermore, some extended emission might be resolved out, and missed, by the FIRST maps.

In the left panel of Fig. 3, we show the distribution of the flux density at 1.4 GHz (i.e.,  $F_{1.4}$ ) for all the sources belonging to the FRICAT; this flux density peaks at  $\sim 50 \text{ mJy}$  and extends up to  $\sim 5 \text{ Jy}$ . The brightest source, FRICAT 1416+1048, is the only objects belonging to the 3C sample, 3C 296. Below the peak the sources density decreases and there are only two objects between 5 and 10 mJy. This flux distribution indicates that indeed the completeness limit of FRICAT is higher than the original 5 mJy and can be set at  $\sim 50 \text{ mJy}$ .

As for the optical selection of the sample, according to Montero-Dorta & Prada (2009), the redshift completeness of the SDSS decreases with decreasing apparent magnitude, starting from  $\sim 90\%$  at the SDSS spectroscopic limit of  $r = 17.77$  and reaching  $\sim 50\%$  at  $r = 11.75$ . Most of the incompleteness is due to the SDSS fiber cladding, which prevents fibers on any given plate from being placed closer than  $55''$  apart. For brighter (and more extended) objects other effects become important, such as the superposition of bright saturated stars on the target.

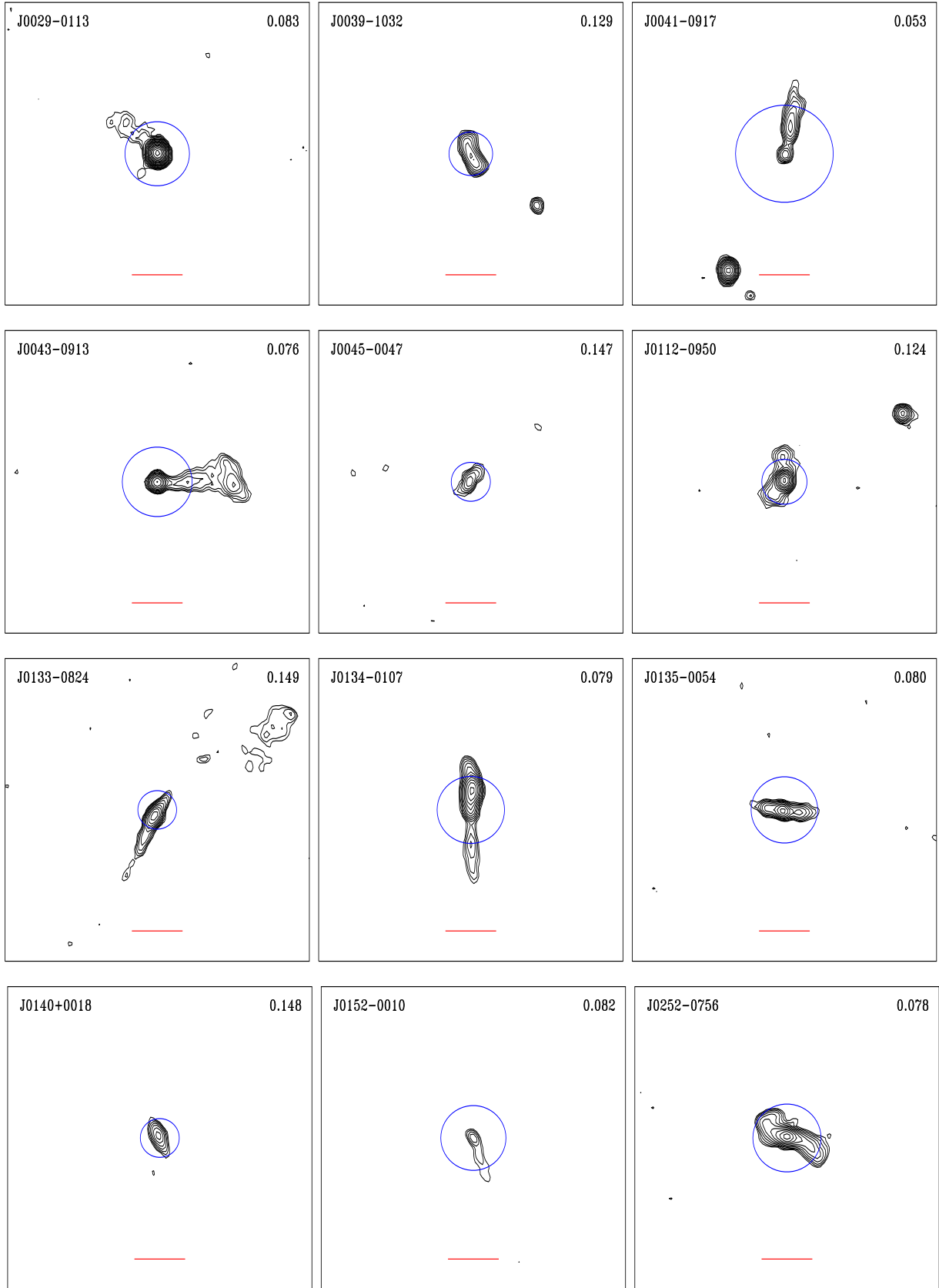


**Fig. 1.** FIRST images of the first 12 FRICAT sources. Contours, corrected for cosmological effects to a redshift of  $z = 0.15$ , are drawn starting from 0.45 mJy/beam and increase with a geometric progression with a common ratio of  $\sqrt{2}$ . The field of view is  $3' \times 3'$ ; the red tick at the bottom is  $30''$  long. The blue circle is centered on the host galaxy and has a radius of 30 kpc. The sources FRICAT name and redshift are reported in the upper corners.

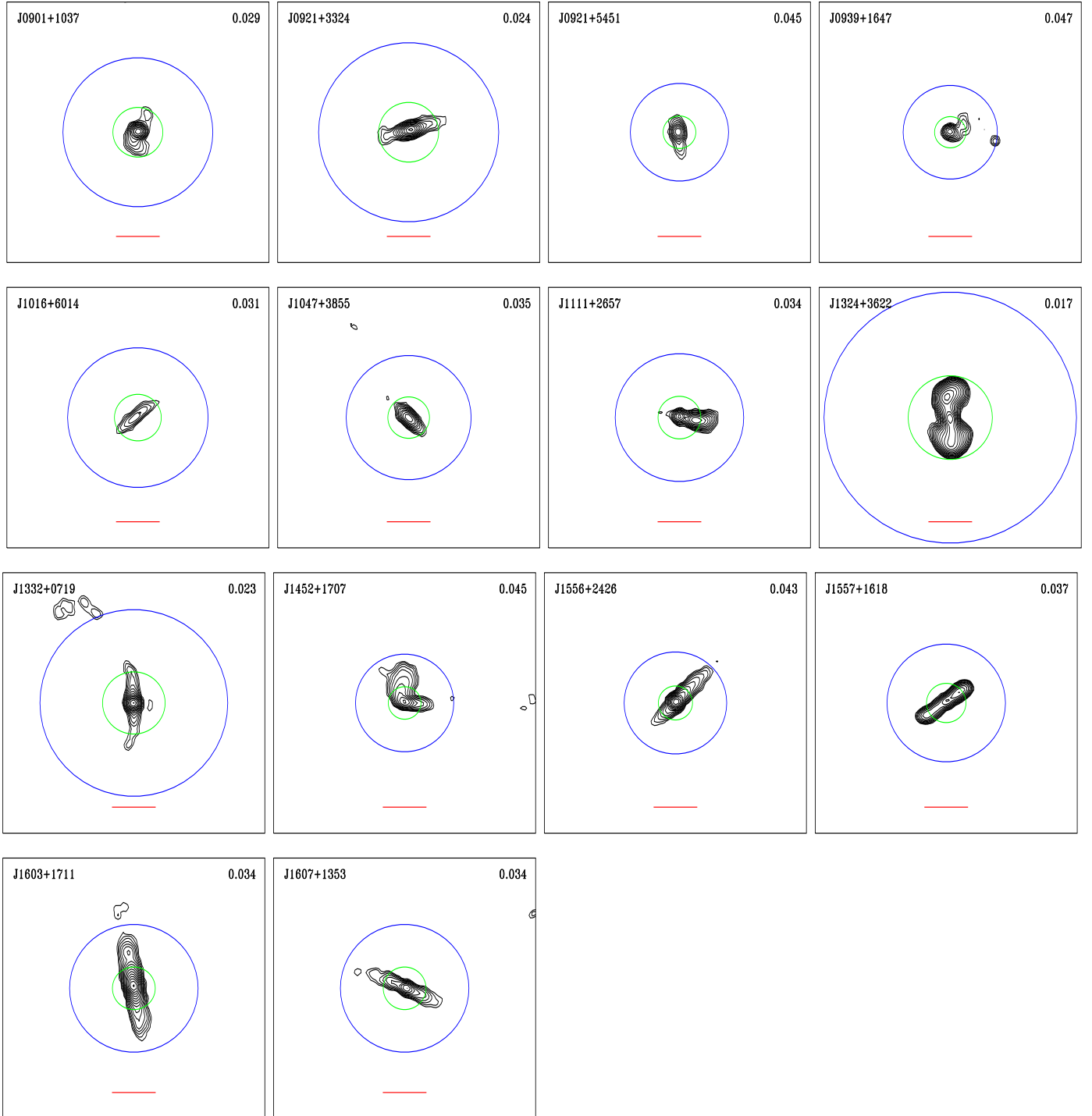


**Fig. 2.** FIRST images of the 14 sFRICAT sources selected at  $z < 0.05$  and extended between 10 and 30 kpc. The green (blue) circle is centered on the host galaxy and has a radius of 10 (30) kpc. The sources sFRICAT name and redshift are reported in the upper corners.

In the right panel of Fig. 3, we show the distribution of the  $r$  magnitude of the FRICAT hosts. The vast majority of them fall in the magnitude range of the SDSS main galaxies sample (Strauss et al. 2002;  $17.77 < r < 14.5$ ); a bright tail of objects (also including most of the sFRICAT hosts) is present but it drops to zero well before the redshift completeness is significantly reduced.

Thus both FR Is catalogs (FRICAT and sFRICAT) are statistically complete at level of  $\sim 90\%$  in the optical energy range. However, it is worth mentioning that this extremely low level

of incompleteness is only due to a random loss of  $\sim 10\%$  of the potential spectroscopic targets (see, e.g., Zehavi et al. 2002).

## 4. FRICAT hosts and radio properties

### 4.1. Hosts properties

All selected FR Is are classified as low excitation galaxies (LEG) by Best & Heckman (2012) based on the ratios of the optical emission lines in their SDSS spectra. There are only four exceptions and these are sources that cannot be classified

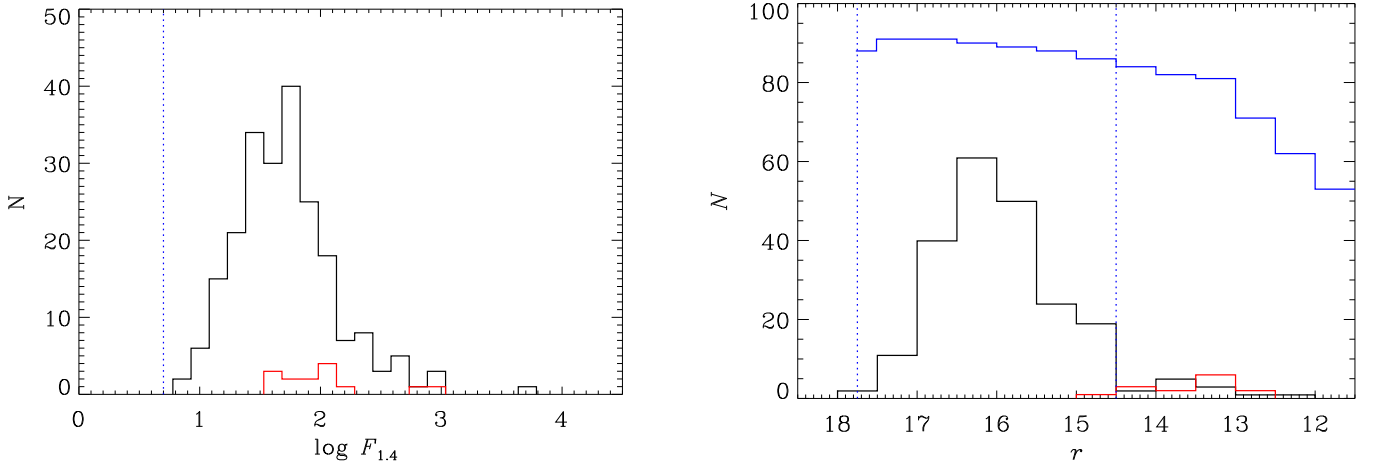


**Fig. 3.** *Left:* distribution of the NVSS fluxes of the 219 FRICAT sources; the red histogram is for the 14 sFRICAT sources. The vertical blue dotted line indicates the 5 mJy limits of the BH12 sample. *Right:* the black curve shows the  $r$ -band magnitude distribution of the FRICAT hosts (the red histogram is for the sFRICAT sources); the vertical dotted lines indicate the limits defining the SDSS main galaxies sample. The blue histogram report the SDSS completeness in percentage from [Montero-Dorta & Prada \(2009\)](#).

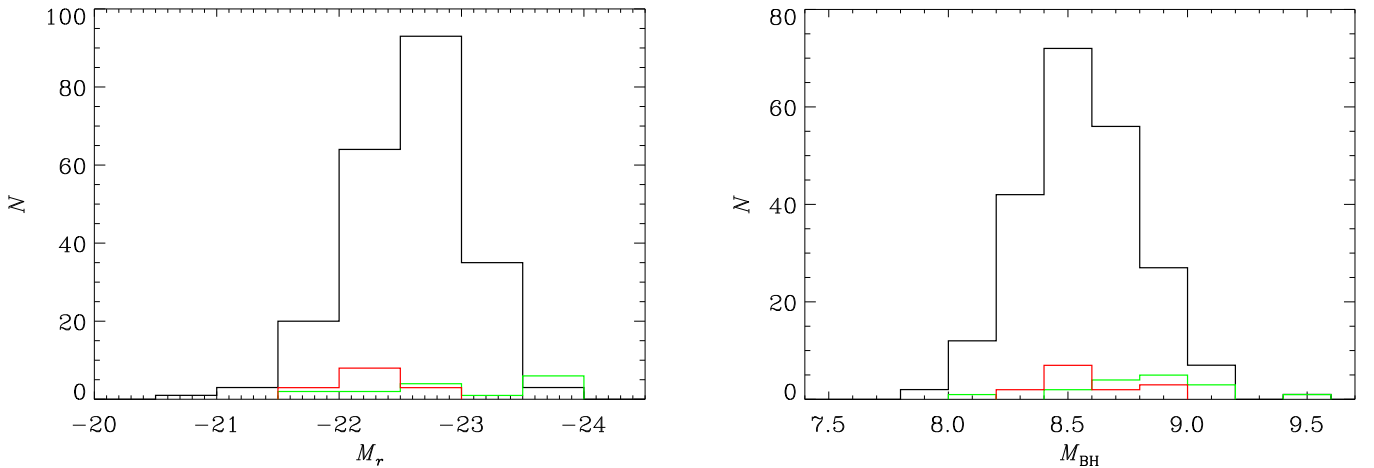


**Fig. 4.** Distributions of the  $r$  band absolute magnitude (*left*) and black hole masses (*right*), black for FRICAT, red for the sFRICAT, and green for the 3C-FRIs.

spectroscopically because some of the diagnostic emission lines cannot be measured in their spectra (see Tables B.1 and B.2); based on the criteria used by [Best & Heckman \(2012\)](#) their radio emission is powered by an AGN. Furthermore, [Baldi & Capetti \(2010\)](#) show that the spectroscopically unclassified objects likely belong to the class of LEG, but with an even lower contrast of the AGN against the host galaxy emission.

The distribution of absolute magnitude of the FRICAT hosts covers the range  $-21 \gtrsim M_r \gtrsim -24$  with a maximum at  $M_r \sim -22.5$  (see Fig. 4, left panel). The distribution of black hole masses (Fig. 4, right panel) covers the range  $8.0 \leq \log M_{\text{BH}} \leq 9.5 M_{\odot}$ , peaking at  $\sim 10^{8.5} M_{\odot}$ .

Various diagnostics can be used for a morphological and spectroscopic classification of the hosts.

The concentration index  $C_r$  is defined as the ratio of the radii including 90% and 50% of the light in the  $r$  band, respectively. Early-type galaxies (ETGs) have higher values of  $C_r$  than late-type galaxies. Two thresholds have been suggested to define ETGs: a more conservative value at  $C_r \gtrsim 2.86$  ([Nakamura et al. 2003](#); [Shen et al. 2003](#)) and a more relaxed selection at  $C_r \gtrsim 2.6$  ([Strateva et al. 2001](#); [Kauffmann et al. 2003](#); [Bell et al. 2003](#)). [Bernardi et al. \(2010\)](#) found that the second threshold of the concentration index corresponds to a mix of E+S0+Sa types,

while the first mainly selects elliptical galaxies, removing the majority of Sacs, but also some Es and S0s.

The Dn(4000) spectroscopic index is defined according to [Balogh et al. \(1999\)](#) as the ratio between the flux density measured on the “red” side of the Ca II break (4000–4100 Å) and that on the “blue” side (3850–3950 Å). Low redshift ( $z < 0.1$ ) red galaxies show  $\text{Dn}(4000) = 1.98 \pm 0.05$ , which is a value that decreases to  $\approx 1.95 \pm 0.05$  for  $0.1 < z < 0.15$  galaxies ([Capetti & Raiteri 2015](#)). The presence of young stars or of non-stellar emission reduces the Dn(4000) index.

In Fig. 5 we show the concentration index  $C_r$  versus the Dn(4000) index (left panel) and versus  $M_{\text{BH}}$  (right panel) for the FRICAT sources. The vast majority of the hosts lie in the region of high  $C_r$  and Dn(4000) values, indicating that they are red ETGs. There are only a few exceptions: FRICAT 0735+4158 has a low concentration index ( $C_r = 2.29$ ), but this is due to the presence of two compact sources close to the host center. FRICAT 1053+4929, FRICAT 1428+4240, and FRICAT 1518+0613 instead have a low Dn(4000) index,  $\sim 1.3$ ; their spectra are rich in absorption lines, suggesting a dilution from nonstellar continuum rather than young stars. Indeed all three sources (that we keep in FRICAT) are included in the list of low luminosity BL Lacs compiled by [Capetti & Raiteri \(2015\)](#).

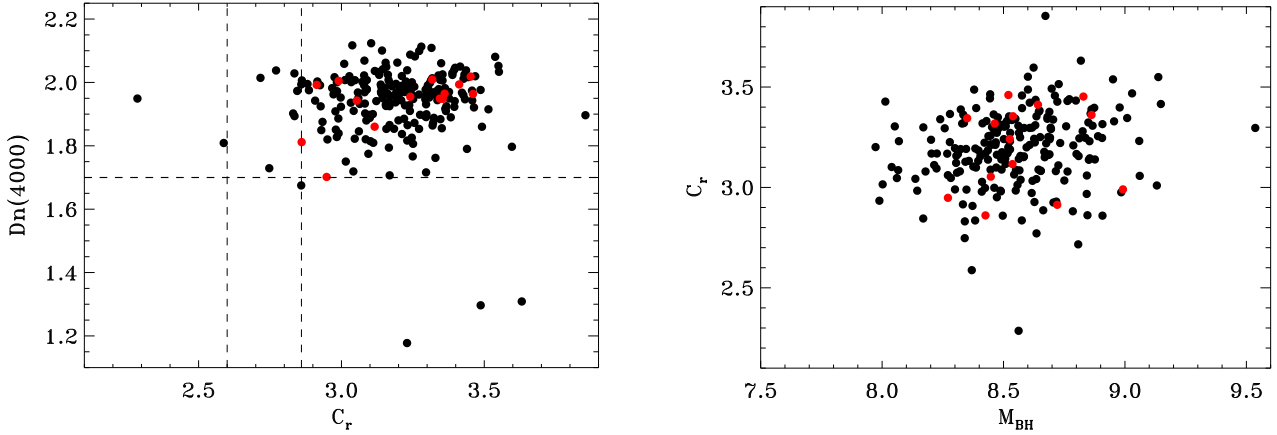


**Fig. 5.** *Left:* concentration index  $C_r$  vs.  $Dn(4000)$  index for the FRICAT and the sFRICAT samples (red dots). *Right:* logarithm of the black hole mass (in solar units) vs. concentration index  $C_r$ .

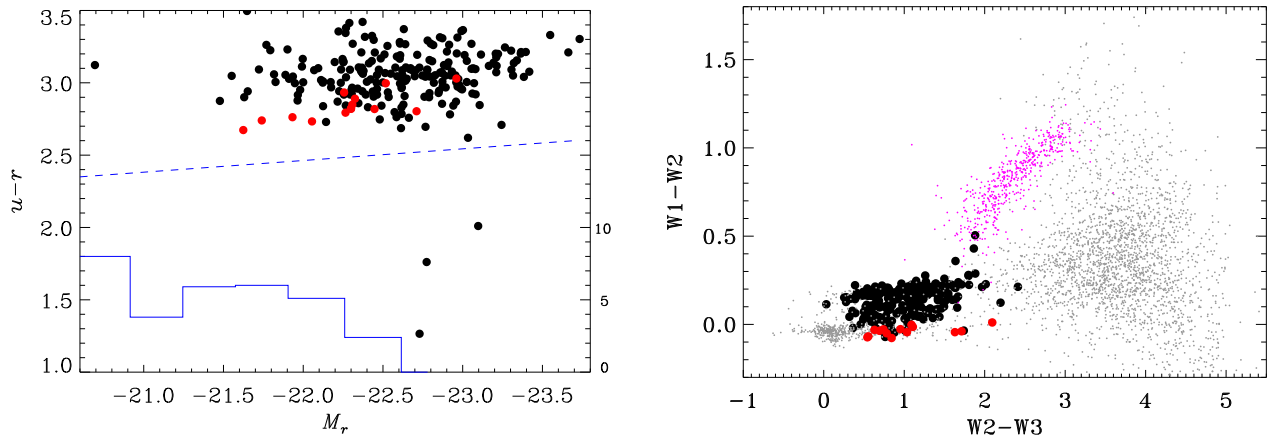


**Fig. 6.** *Left:* absolute  $r$  band magnitude,  $M_r$ , vs.  $u-r$  color for the FRICAT hosts (the red dots represent the sFRICAT sample). The blue histogram on the bottom shows the percentage of blue ETGs (scale on the right axis) from Schawinski et al. (2009). The dashed line separates the “blue” ETG from the red sequence, following their definition. *Right:* WISE mid-IR colors of the FRICAT hosts compared to those of  $\sim 3000$  randomly selected IR sources (gray dots) selected at high Galactic latitudes. We also show the region occupied by the *Fermi* blazars (purple dots).

The  $Dn(4000)$  index refers only to the region covered by the SDSS spectroscopic aperture,  $3''$  in diameter. In order to explore the global properties of the FRICAT hosts, we also consider the  $u-r$  color of the galaxies as a whole. In Fig. 6 we show the  $u-r$  color versus the absolute  $r$ -band magnitude  $M_r$  of the hosts. With the exception of the three BL Lacs, they are all located above the line separating red and blue ETGs. The fraction of “blue” ETGs (represented as the histogram at the bottom of the figure) decreases with increasing luminosity and these ETGs disappear for  $M_r \lesssim -22.5$  (Schawinski et al. 2009). The lack of blue ETGs among the FRICAT hosts is relevant; however, their expected number, based on their  $M_r$  distribution and the “blue” fraction of the general ETGs population, is only 4.3.

The WISE infrared colors further support the passive nature of the FRICAT hosts. In Fig. 6 we show the comparison between the mid-IR colors of FRICAT sources and those of  $\sim 3000$  randomly selected sources (gray circles) at high Galactic latitudes (i.e.,  $|b| > 40^\circ$ ). The associations between the FRICAT and the WISE catalog were computed adopting a  $3'3$  angular separation, which corresponds to the combination of the typical positional uncertainty of the WISE all sky survey (Wright et al. 2010) and that of the FIRST (D’Abrusco et al. 2014). Fifty-seven of them are undetected in the W3 band and these objects are not reproduced in the figure. In the same figure we also report the mid-IR colors of the *Fermi* blazars for reference of

WISE sources whose IR emission is dominated by nonthermal radiation (Massaro et al. 2011; D’Abrusco et al. 2012). FRICAT sources appear to have mid-IR colors mostly dominated by their host galaxies (they fall in the same region as elliptical galaxies; Wright et al. 2010) and not contaminated by the emission of their jets. Only the three BL Lacs have  $W2-W3 > 0.3$  and they are located at the onset of the sequence defined by the more luminous objects of this class (Massaro et al. 2012).

#### 4.2. Radio properties

The distribution of radio luminosity at 1.4 GHz of the FRICAT covers the range  $L_{1.4} = \nu_r I_r = \sim 10^{39.5} - 10^{41.3}$  erg s $^{-1}$  those of the sFRICAT sample instead have  $10^{39} \lesssim L_{1.4} \lesssim 10^{40.4}$  erg s $^{-1}$ . The Fanaroff & Riley (1974) separation between FR Is and FR IIs translates, with our adopted cosmology and by assuming a spectral index of 0.7 between 178 MHz and 1.4 GHz, into  $L_{1.4} \sim 10^{41.6}$  erg s $^{-1}$ . All objects included in our sample fall below this threshold, although it must be kept in mind that the power separation between FR Is and FR IIs is sharper at 178 MHz than at higher frequencies (Zirbel & Baum 1995).

The separation between FR classes is cleaner in the optical-radio luminosity plane (Ledlow & Owen 1996). Indeed, the bulk of the FRICAT sources lie below the boundary between FR I and FR II reported by Ledlow & Owen (see left panel Fig. 7) in the region populated by FR I sources. Be aware that we shifted

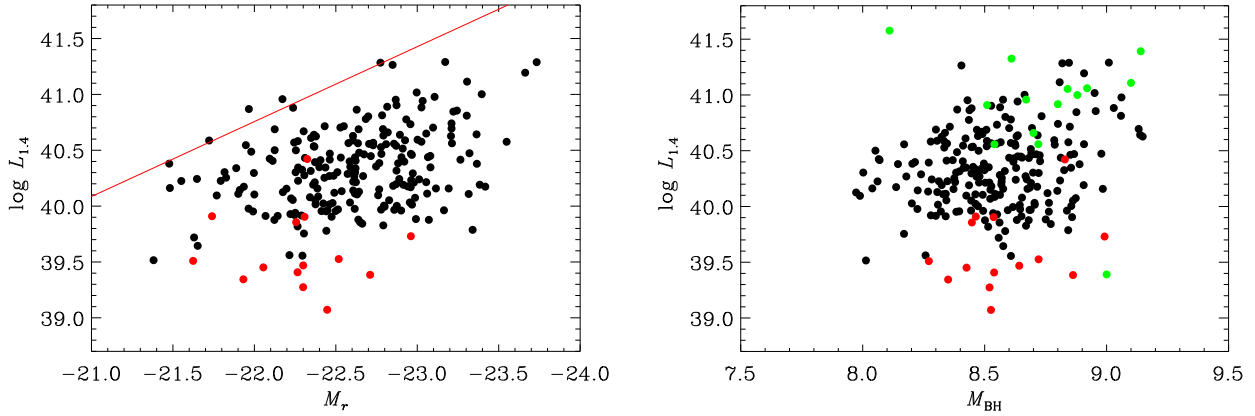


**Fig. 7.** *Left panel:* radio luminosity (NVSS) vs. host absolute magnitude,  $M_r$ , for FRICAT and sFRICAT (black and red, respectively). The solid line shows the separation between FR I and FR II reported by Ledlow & Owen (1996) to which we applied a correction of 0.34 mag to account for the different magnitude definition and the color transformation between the SDSS and Cousins systems. *Right panel:* radio luminosity vs. black hole mass. The green points are the 3C-FR Is.

the dividing line to the right of the diagram to include a correction of 0.12 mag to scale our total magnitude to the  $M_{24.5}$  used by these authors, and an additional 0.22 mag to convert the Cousins system into the SDSS system (Fukugita et al. 1996). This confirms the indication that more powerful FR Is can be associated with more massive galaxies, while in less luminous hosts the FR I/FR II transition occurs at lower  $L_{1.4}$ ; as a result, a positive trend links  $L_{1.4}$  and  $M_r$ . A similar trend is seen also between  $L_{1.4}$  and  $M_{\text{BH}}$  (Fig. 7, right panel). This is likely to be driven by the connection between  $M_{\text{BH}}$  and the host luminosity (Marconi & Hunt 2003) combined with the Ledlow & Owen effect.

FR Is show a large spread in both radio and [O III] line luminosities (see Fig. 8), both quantities spanning over two orders of magnitude. The FR Is of the sFRICAT sample fall generally in the low end of the radio luminosity distribution. Within the same volume ( $z < 0.05$ ), the sources extending to  $10 < r < 30$  kpc have a median luminosity that are four times smaller than those with  $r > 30$  kpc.

## 5. Discussion

The population of the FRICAT hosts is remarkably uniform. They are all luminous red ETGs, with large black hole masses ( $M_{\text{BH}} \gtrsim 10^8 M_{\odot}$ ), spectroscopically classified as LEGs. All these properties are shared with the hosts of the “small” FR Is and the more powerful 3C-FR Is. We included in the 3C-FR Is sample the 16 radio galaxies with  $z < 0.3$  and a FR I morphology, according to Buttiglione et al. (2010), and with either a direct  $M_{\text{BH}}$  measurement or a published stellar velocity dispersion in the HyperLeda database<sup>2</sup>. More quantitatively, the distributions of  $M_{\text{BH}}$  and  $M_r$  of the FRICAT and sFRICAT samples are not statistically distinguishable, according to the Kolmogoroff-Smirnov test. A small difference might instead emerge when considering the 3C-FR Is hosts. This latter sample has a median  $M_{\text{BH}}$  that is a factor of 1.9 higher with respect to the FRICAT (and they are 0.2 mag brighter). As discussed in the previous section, this might be the manifestation of the Ledlow & Owen effect. Nonetheless, the null hypothesis that they are drawn from different populations cannot be rejected at a  $3\sigma$  confidence level.

Even though the hosts of three FR Is samples are very similar, the FRICAT sources show a very different properties with

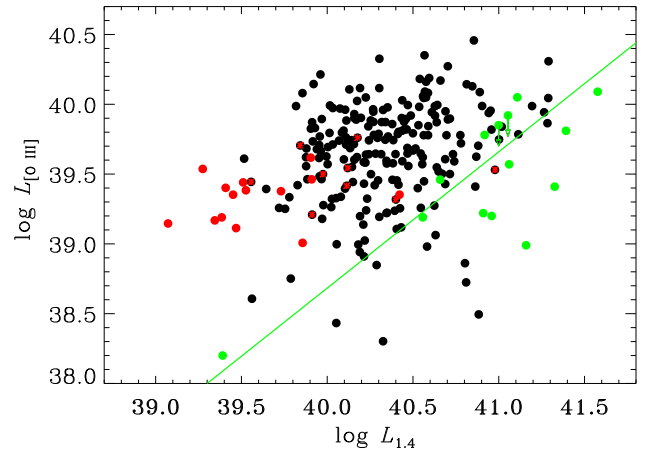


**Fig. 8.** Radio (NVSS) vs. [O III] line luminosity of the FRICAT, sFRICAT, and 3C-FR I samples (black, red, and green points, respectively). The FRICAT sources with  $z < 0.05$  are represented as black dots with a red asterisk superimposed. The green line shows the linear correlation between these two quantities derived from the FR Is of the 3C sample from (Buttiglione et al. 2010).

respect to what is seen in the 3C sample for the connection between emission lines and radio luminosities.

The 3C-FR Is show a positive trend between the line and radio luminosities with a slope consistent with unity (e.g., Buttiglione et al. 2010). This indicates that a constant fraction of the AGN power, as measured from the emission lines, is converted into radio emission. Buttiglione et al. show that the same result, although with a different normalization, is found when considering the 3C-FR II radio galaxies.

Conversely, no correlation between  $L_{1.4}$  and  $L_{[\text{O III}]}$  can be seen for the FRICAT where, at a given line luminosity, the radio luminosities span over two orders of magnitude. Similar to what is seen in the 3C sample, it appears that no source has a  $L_{1.4}/L_{[\text{O III}]}$  ratio exceeding  $\sim 100$ , producing the scarcely populated region in the bottom right portion of this diagram; but objects are found with much lower ratios down to  $L_{1.4}/L_{[\text{O III}]} \sim 0.5$ . Furthermore, the radio luminosity grows, not surprisingly, when the size of the radio source increases. Less obviously, the FR Is in the “small” sample have a lower (by a factor of  $\sim 3$ ) median ratio between line and radio luminosity.

Apparently, the high flux threshold used for the selection of the 3C sources favored the inclusion of radio galaxies with high

<sup>2</sup> <http://leda.univ-lyon1.fr/>

ratios between radio and optical luminosity. A much larger population of FR Is emerges when lowering the radio flux limit by three orders of magnitude. The connection between radio and line luminosity disappears. The spectroscopic and host properties of the FR I hosts rule out the possibility of a substantial contribution to the [O III] line by star formation that might compromise our ability to reveal this trend, if indeed this was present. The broad distribution of  $L_{1.4}/L_{[\text{O III}]}$  ratio indicates a corresponding broad range of conversion of AGN bolometric power into radio emission.

## 6. Summary and conclusions

We built a catalog of 219 FR I radio galaxies, called FRICAT, selected from the Best & Heckman (2012) sample, and obtained by combining the SDSS, NVSS, and FIRST surveys.

The FR I classification is purely morphological and based on the visual inspection of the FIRST radio images. We included the sources in which the radio emission reaches a distance of at least 30 kpc from the host (restricting the analysis to those with redshift  $z < 0.15$ ). We adopted rather strict criteria for a positive FR I classification; we selected only sources showing one-sided or two-sided jets in which the surface brightness is generally decreasing along its whole length, lacking of any brightness enhancement at the jet end, i.e., with an edge-darkened structure. The resulting FRICAT catalog comprises 219 objects. A second sample of 14 objects, sFRICAT, extends the selection to smaller FR Is by including sources with  $10 < r < 30$  kpc and  $z < 0.05$ .

These samples have a high level of completeness (~90%) in both their radio and optical selection. As such, they can be used to study, for example, their radio and bivariate radio/optical luminosity functions. One should nonetheless bear in mind the morphological selection criteria adopted and that the completeness limit in the radio band is ~50 mJy. These are well suited for our purposes but it will be certainly interesting to explore the connection of the FRICAT with the remaining ~500 extended radio galaxies we did not include in our analysis.

The FRICAT hosts are remarkably homogeneous, as they are all luminous red ETGs with large black hole masses that are spectroscopically classified as LEGs. All these properties are shared by the hosts of more powerful FR Is in the 3C sample. They do not show significant differences from the point of view of their colors with respect to the general population of massive ETGs. The presence of an active nucleus (and its level of activity) does not appear to affect the hosts of FR Is.

The FRICAT sources differ from the 3C-FRIs for the connection between emission lines and radio luminosities. While in 3C-FRIs the line and radio luminosities are correlated (suggesting that a constant fraction of the AGN power is converted into radio emission) these two quantities are unrelated in the FRICAT. We argue that the line/radio correlation is the result of a selection bias because of the high flux threshold of the 3C sources that favors the inclusion of radio galaxies with high ratios between radio and optical luminosity. Baldi & Capetti (2009) reached a similar conclusion from the comparison of the 3C objects with the radio galaxies associated with nearby ( $z \lesssim 0.01$ ) optically luminous ETGs.

The 3C-FRIs represent the tip of the iceberg of a much larger and diverse population of FR Is. This result highlights the importance of exploring a broader (and larger) population of FR Is. Several other issues, such as those listed in the Introduction, can now be addressed by using FRICAT. In particular we will explore in two forthcoming papers the environment of FRICAT and how they are related to the class of the compact FR 0 radio sources (Baldi et al. 2015).

*Acknowledgements.* F.M. gratefully acknowledges the financial support of the Programma Giovani Ricercatori – Rita Levi Montalcini – Rientro dei Cervelli (2012) awarded by the Italian Ministry of Education, Universities and Research (MIUR). Part of this work is based on the NVSS (NRAO VLA Sky Survey): The National Radio Astronomy Observatory is operated by Associated Universities, Inc., under contract with the National Science Foundation. This publication makes use of data products from the Wide-field Infrared Survey Explorer, which is a joint project of the University of California, Los Angeles, and the Jet Propulsion Laboratory/California Institute of Technology, funded by the National Aeronautics and Space Administration. This research made use of the NASA/IPAC Infrared Science Archive and Extragalactic Database (NED), which are operated by the Jet Propulsion Laboratory, California Institute of Technology, under contract with the National Aeronautics and Space Administration. We acknowledge the usage of the HyperLeda database (<http://leda.univ-lyon1.fr>). Funding for SDSS-III has been provided by the Alfred P. Sloan Foundation, the Participating Institutions, the National Science Foundation, and the US Department of Energy Office of Science. The SDSS-III web site is <http://www.sdss3.org/>. SDSS-III is managed by the Astrophysical Research Consortium for the Participating Institutions of the SDSS-III Collaboration, including the University of Arizona, the Brazilian Participation Group, Brookhaven National Laboratory, University of Cambridge, Carnegie Mellon University, University of Florida, the French Participation Group, the German Participation Group, Harvard University, the Instituto de Astrofísica de Canarias, the Michigan State/Notre Dame/JINA Participation Group, Johns Hopkins University, Lawrence Berkeley National Laboratory, Max Planck Institute for Astrophysics, Max Planck Institute for Extraterrestrial Physics, New Mexico State University, New York University, Ohio State University, Pennsylvania State University, University of Portsmouth, Princeton University, the Spanish Participation Group, University of Tokyo, University of Utah, Vanderbilt University, University of Virginia, University of Washington, and Yale University.

## References

- Abazajian, K. N., Adelman-McCarthy, J. K., Agüeros, M. A., et al. 2009, *ApJS*, **182**, 543
- Baldi, R. D., & Capetti, A. 2009, *A&A*, **508**, 603
- Baldi, R. D., & Capetti, A. 2010, *A&A*, **519**, A48
- Baldi, R. D., Capetti, A., & Giovannini, G. 2015, *A&A*, **576**, A38
- Balogh, M. L., Morris, S. L., Yee, H. K. C., Carlberg, R. G., & Ellingson, E. 1999, *ApJ*, **527**, 54
- Becker, R. H., White, R. L., & Helfand, D. J. 1995, *ApJ*, **450**, 559
- Bell, E. F., McIntosh, D. H., Katz, N., & Weinberg, M. D. 2003, *ApJS*, **149**, 289
- Bennett, A. S. 1962, *MmRAS*, **68**, 163
- Bernardi, M., Shankar, F., Hyde, J. B., et al. 2010, *MNRAS*, **404**, 2087
- Best, P. N., & Heckman, T. M. 2012, *MNRAS*, **421**, 1569
- Best, P. N., Kauffmann, G., Heckman, T. M., et al. 2005, *MNRAS*, **362**, 25
- Brinchmann, J., Charlot, S., White, S. D. M., et al. 2004, *MNRAS*, **351**, 1151
- Buttiglione, S., Capetti, A., Celotti, A., et al. 2010, *A&A*, **509**, A6
- Capetti, A., & Raiteri, C. M. 2015, *A&A*, **580**, A73
- Colla, G., Fanti, C., Fanti, R., et al. 1975, *A&AS*, **20**, 1
- Condon, J. J., Cotton, W. D., Greisen, E. W., et al. 1998, *AJ*, **115**, 1693
- D’Abrusco, R., Massaro, F., Ajello, M., et al. 2012, *ApJ*, **748**, 68
- D’Abrusco, R., Massaro, F., Paggi, A., et al. 2014, *ApJS*, **215**, 14
- Fanaroff, B. L., & Riley, J. M. 1974, *MNRAS*, **167**, 31
- Fanti, R., Gioia, I., Lari, C., & Ulrich, M. H. 1978, *A&AS*, **34**, 341
- Fukugita, M., Ichikawa, T., Gunn, J. E., et al. 1996, *AJ*, **111**, 1748
- Kauffmann, G., Heckman, T. M., White, S. D. M., et al. 2003, *MNRAS*, **341**, 33
- Ledlow, M. J., & Owen, F. N. 1996, *AJ*, **112**, 9
- Marconi, A., & Hunt, L. K. 2003, *ApJ*, **589**, L21
- Massaro, F., D’Abrusco, R., Ajello, M., Grindlay, J. E., & Smith, H. A. 2011, *ApJ*, **740**, L48
- Massaro, F., D’Abrusco, R., Tosti, G., et al. 2012, *ApJ*, **750**, 138
- Montero-Dorta, A. D., & Prada, F. 2009, *MNRAS*, **399**, 1106
- Nakamura, O., Fukugita, M., Yasuda, N., et al. 2003, *AJ*, **125**, 1682
- Owen, F. N., & Rudnick, L. 1976, *ApJ*, **205**, L1
- Planck Collaboration XIII. 2016, *A&A*, **594**, A13
- Rudnick, L., & Owen, F. N. 1977, *AJ*, **82**, 1
- Schawinski, K., Lintott, C., Thomas, D., et al. 2009, *MNRAS*, **396**, 818
- Shen, S., Mo, H. J., White, S. D. M., et al. 2003, *MNRAS*, **343**, 978
- Strateva, I., Ivezić, Ž., Knapp, G. R., et al. 2001, *AJ*, **122**, 1861
- Strauss, M. A., Weinberg, D. H., Lupton, R. H., et al. 2002, *AJ*, **124**, 1810
- Tremaine, S., Gebhardt, K., Bender, R., et al. 2002, *ApJ*, **574**, 740
- Tremonti, C. A., Heckman, T. M., Kauffmann, G., et al. 2004, *ApJ*, **613**, 898
- Wright, E. L., Eisenhardt, P. R. M., Mainzer, A. K., et al. 2010, *AJ*, **140**, 1868
- Zehavi, I., Blanton, M. R., Frieman, J. A., et al. 2002, *ApJ*, **571**, 172
- Zirbel, E. L., & Baum, S. A. 1995, *ApJ*, **448**, 521

Appendix A: FIRST images of the 219 FRICAT sources

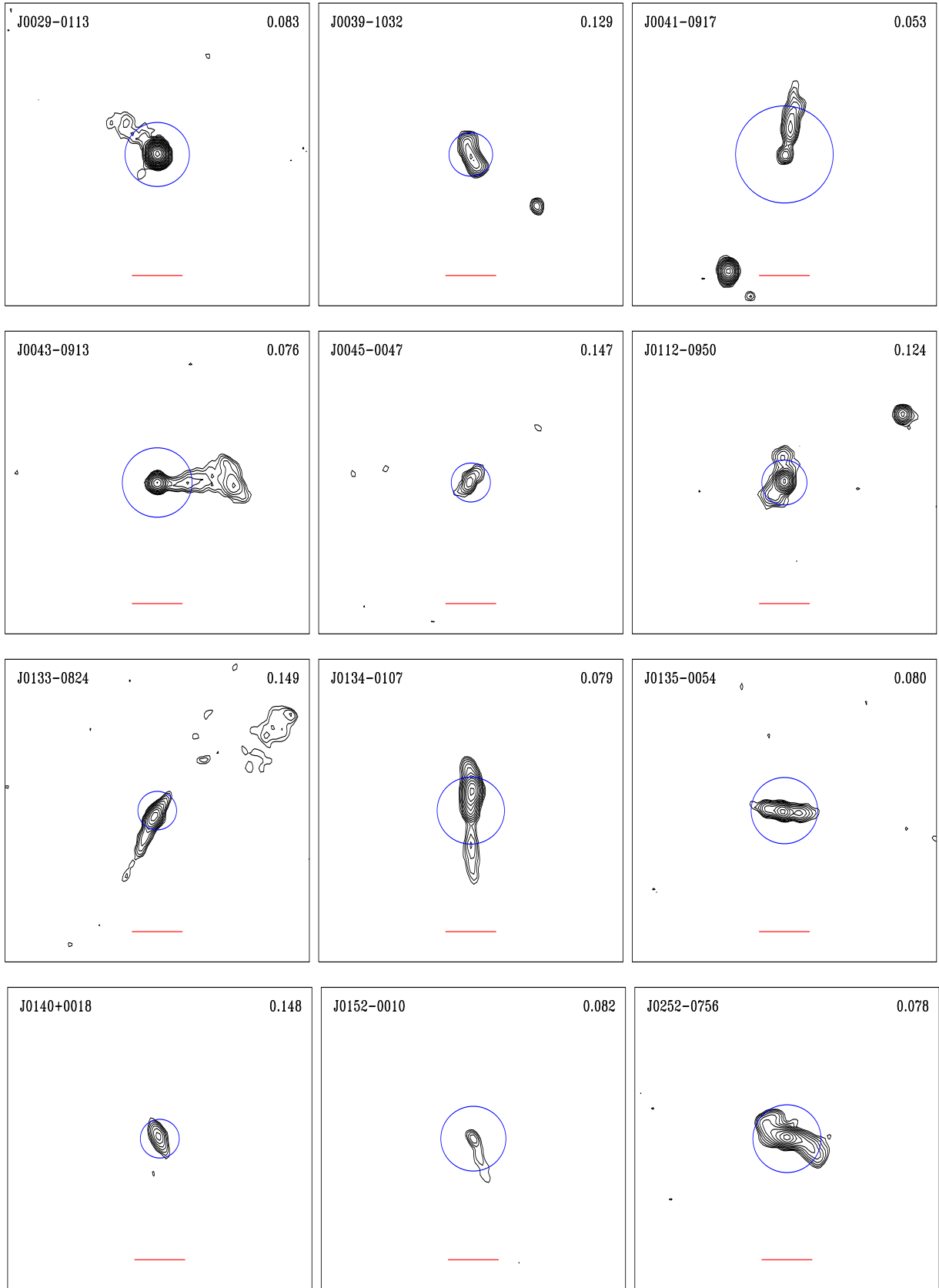


**Fig. A.1.** Images of the FR Is selected. Contours, corrected for cosmological effects to a redshift of  $z = 0.15$ , are drawn starting from 0.45 mJy/beam and increase with a geometric progression with a common ratio of  $\sqrt{2}$ . The field of view is  $3' \times 3'$ ; the red tick at the bottom is 30'' long. The blue circle is centered on the host galaxy and has a radius of 30 kpc. The source ID and redshift are reported in the upper corners.

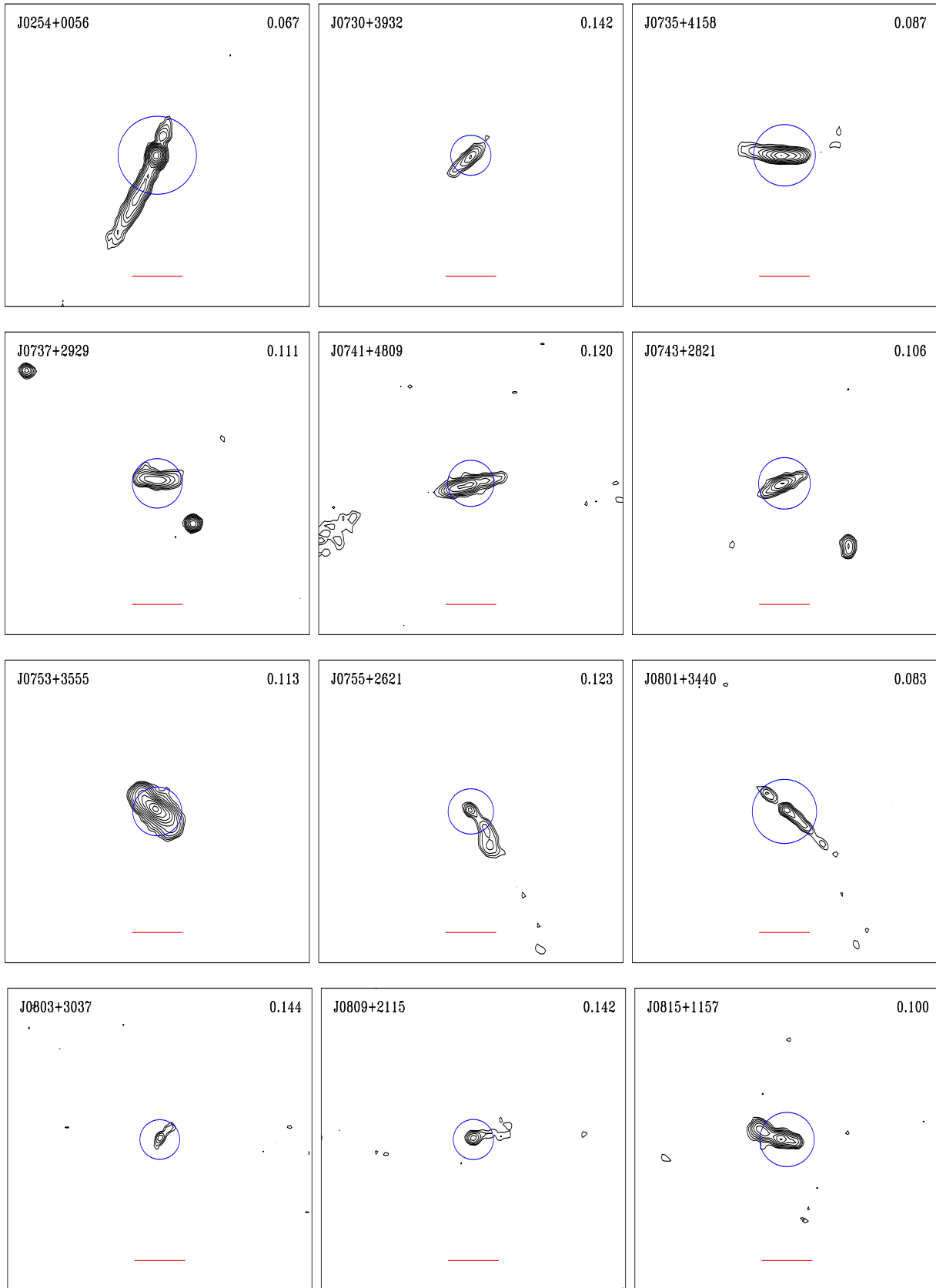


Fig. A.1. continued.

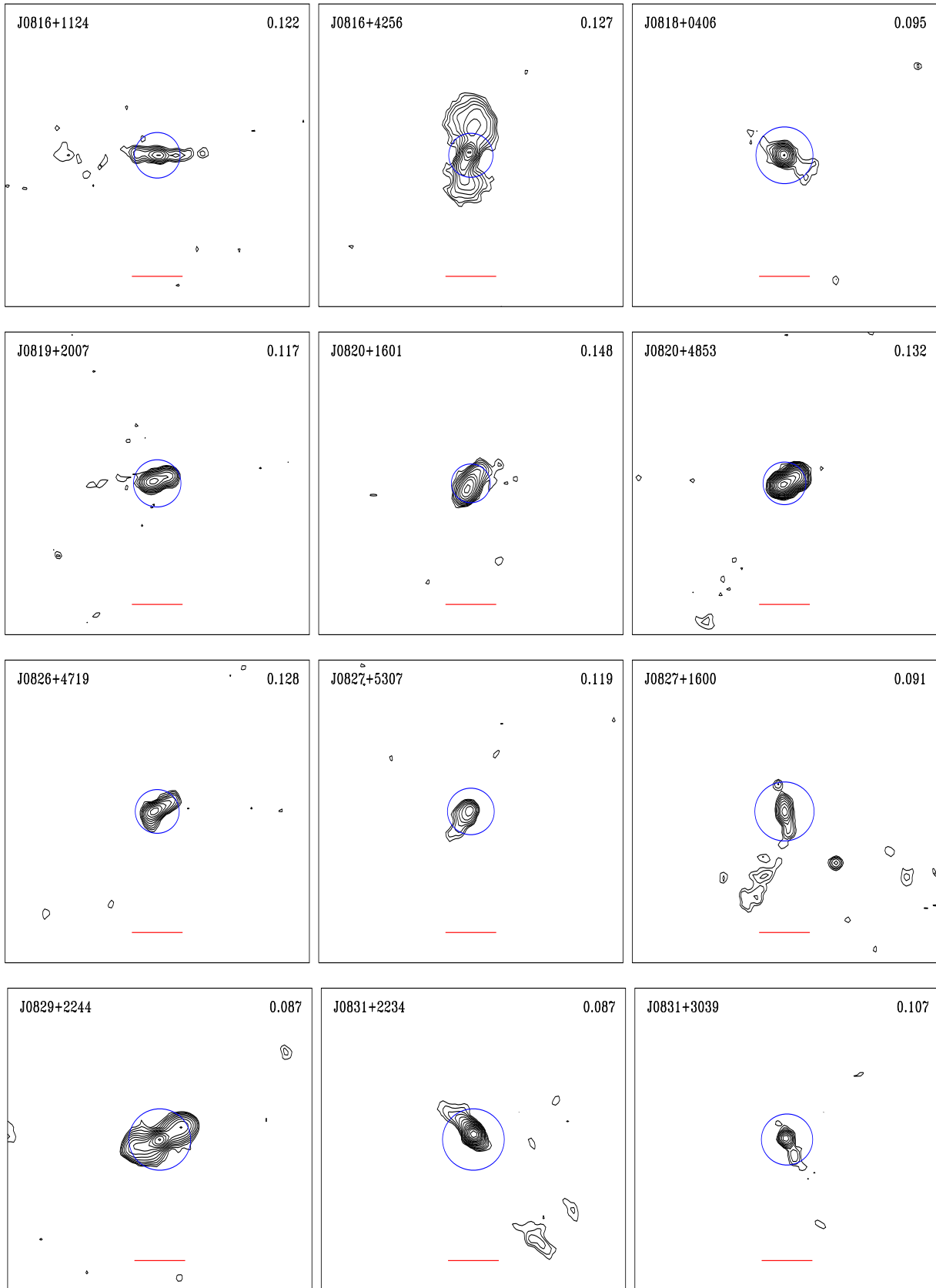


Fig. A.1. continued.

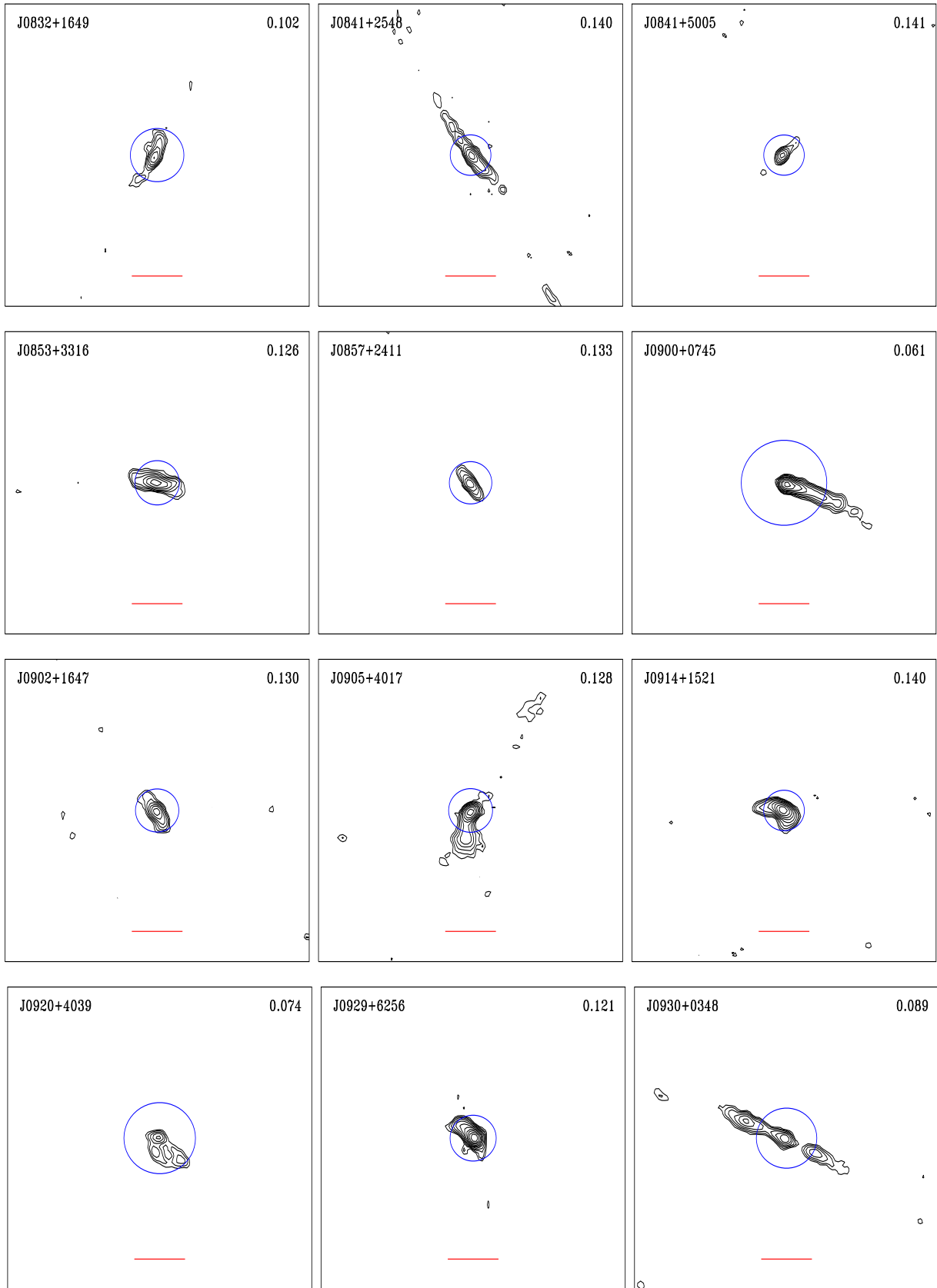


Fig. A.1. continued.

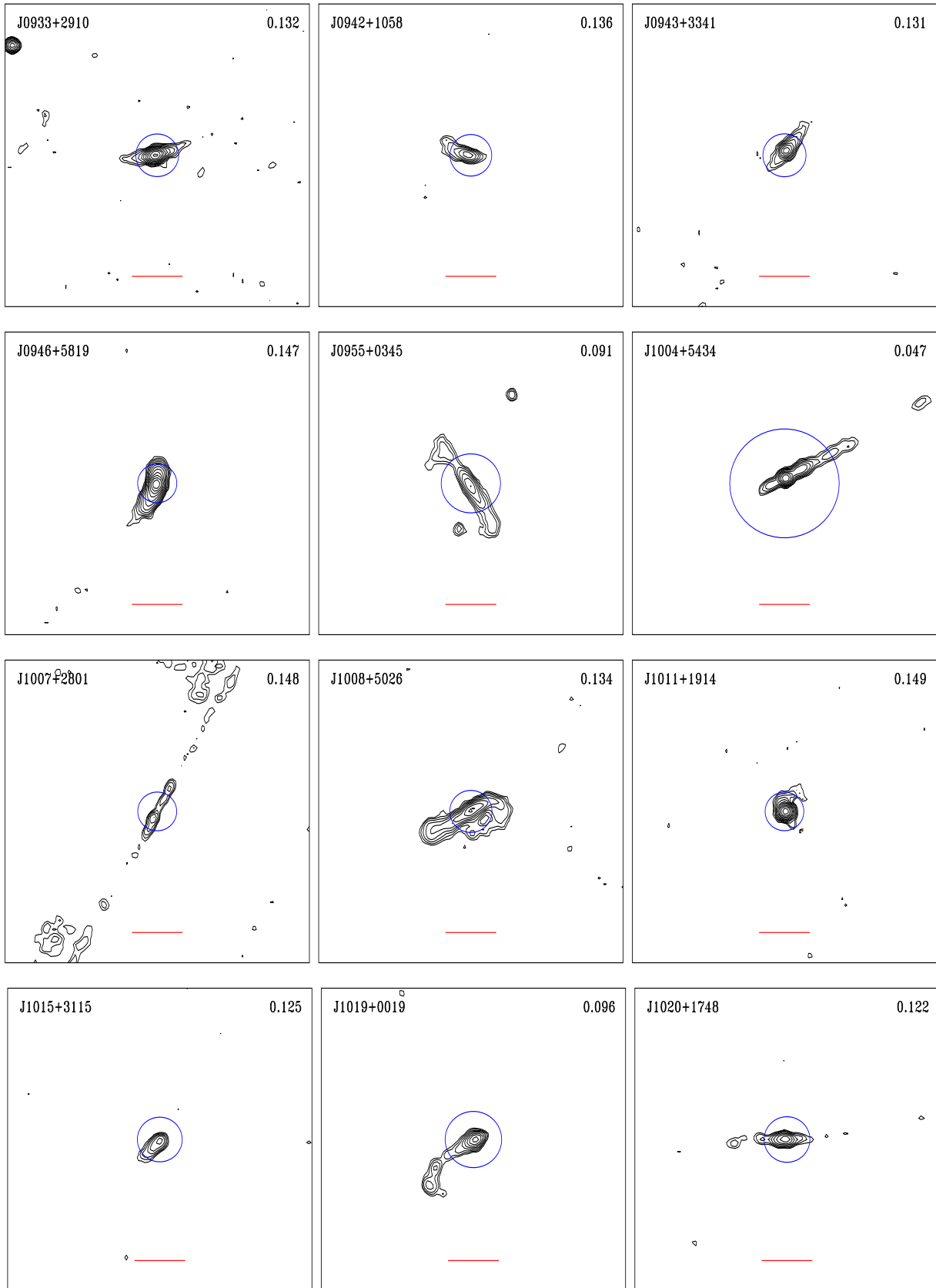


Fig. A.1. continued.

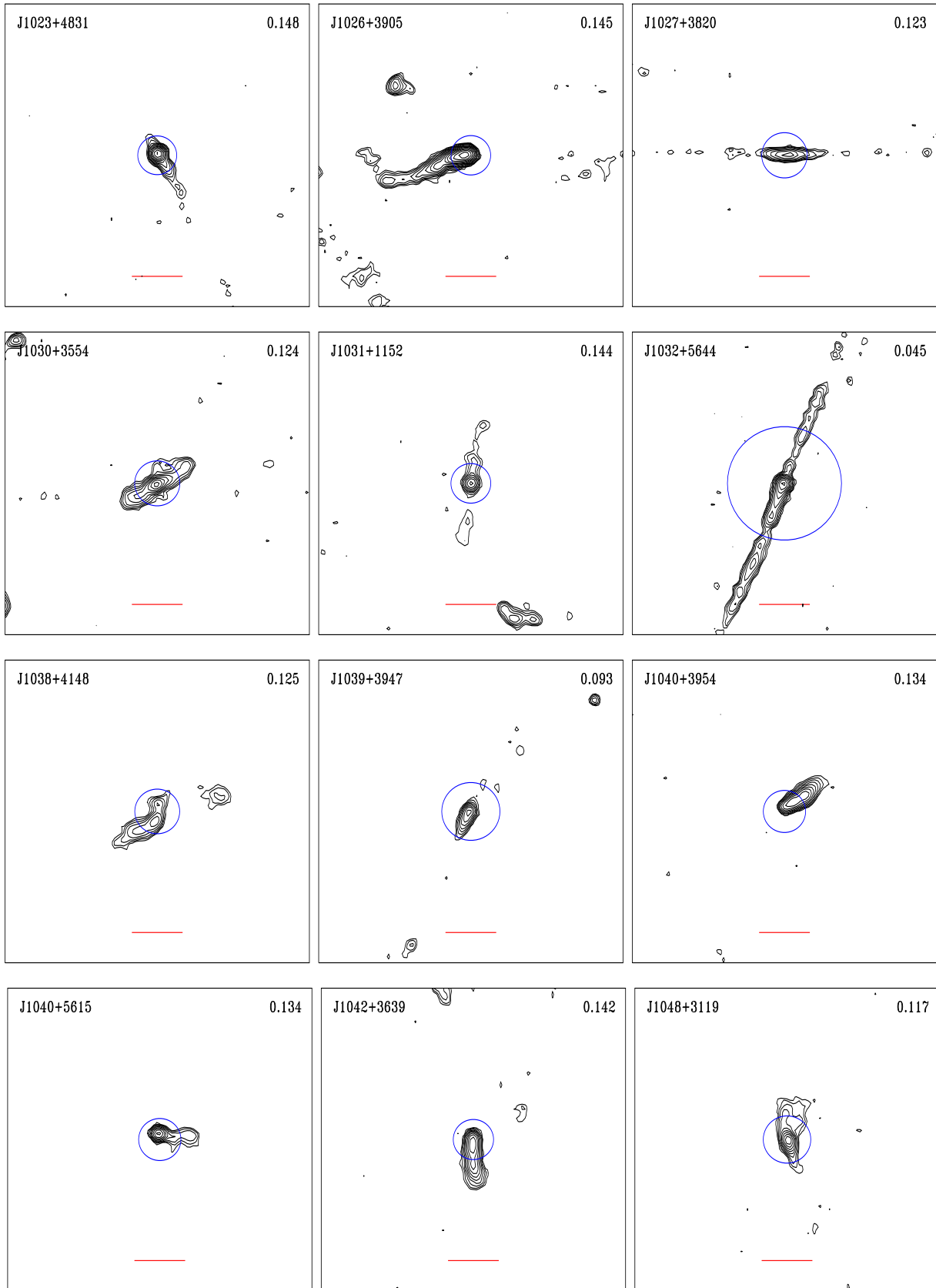


Fig. A.1. continued.

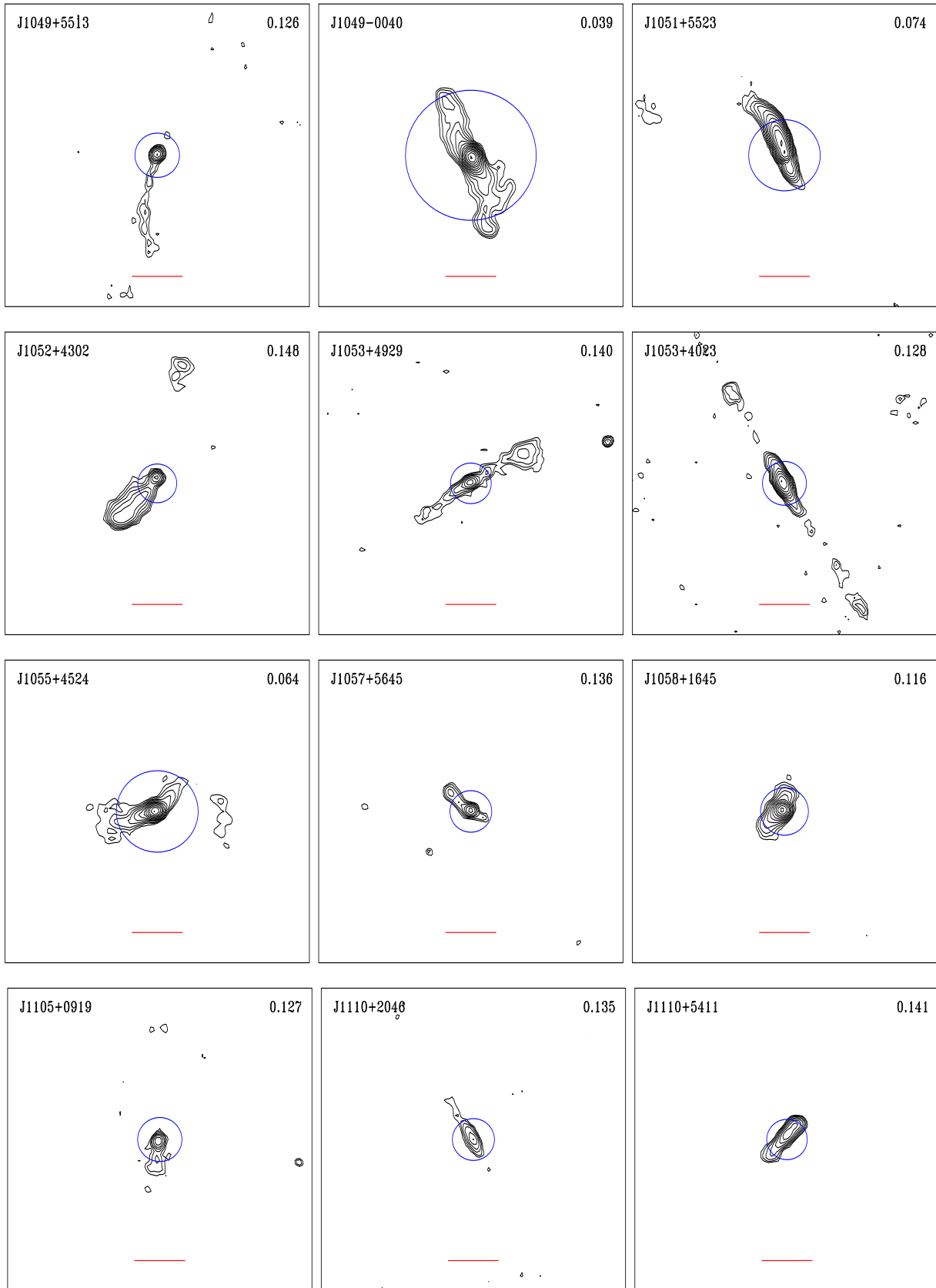


Fig. A.1. continued.

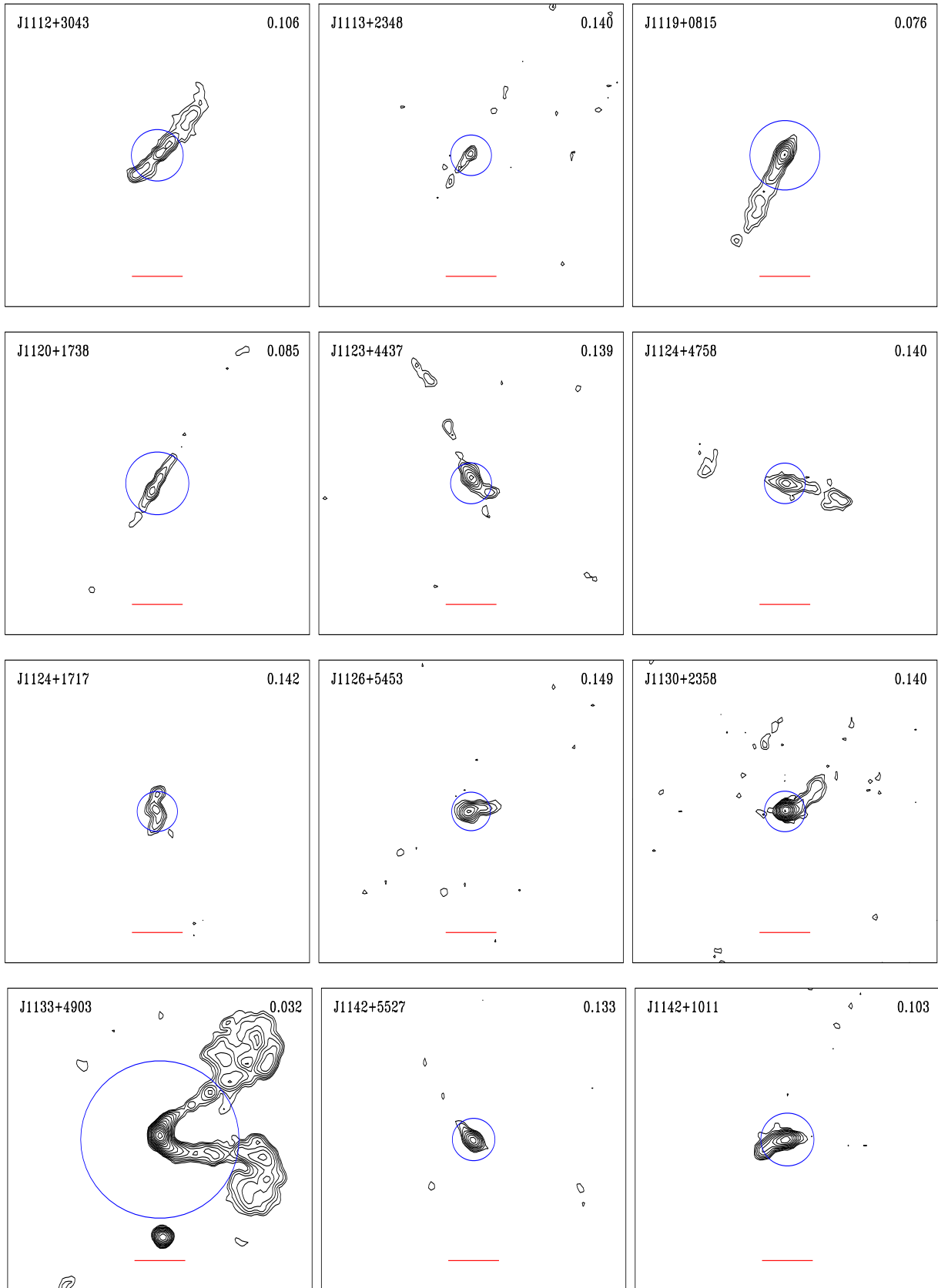


Fig. A.1. continued.

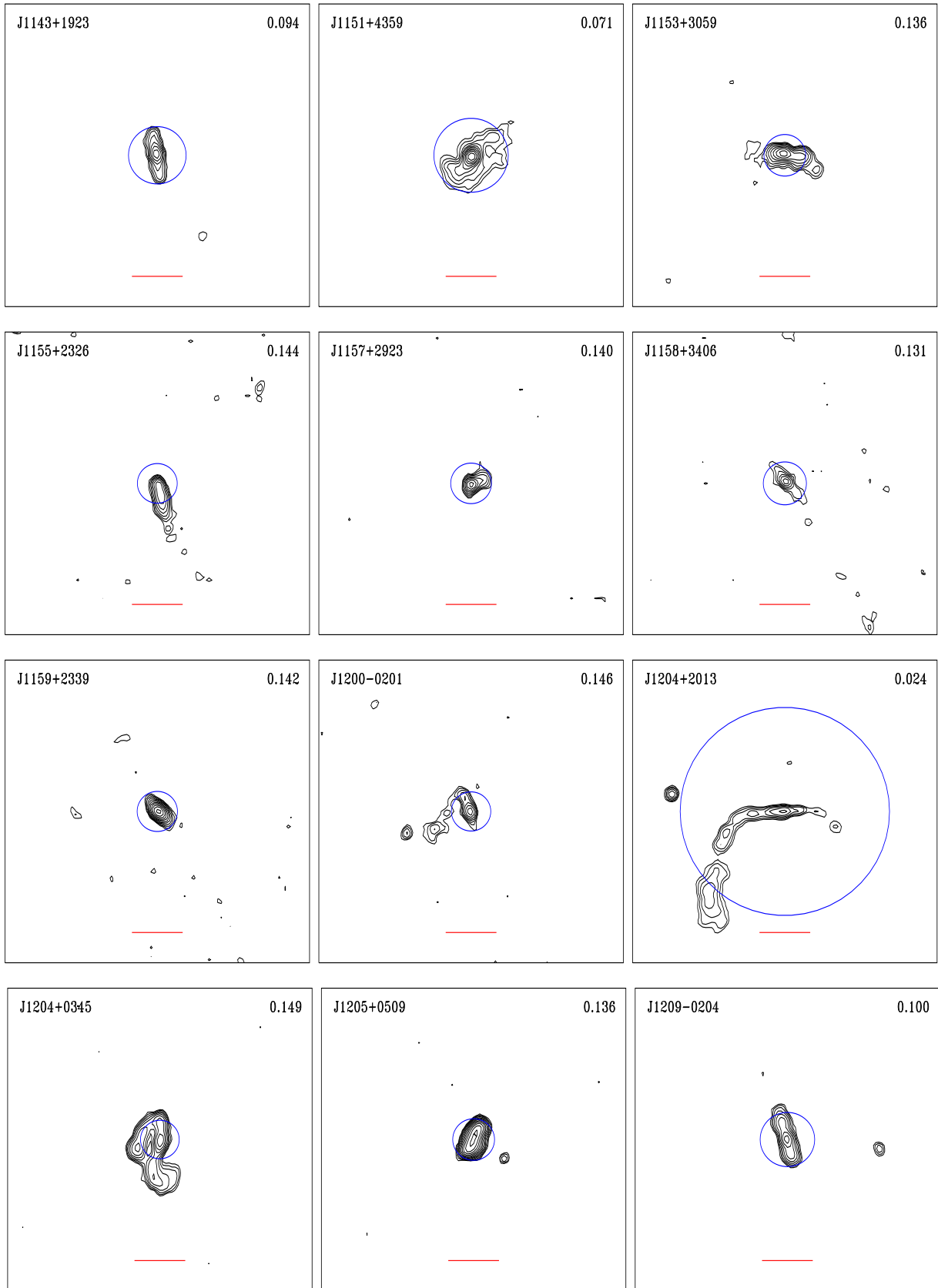


Fig. A.1. continued.

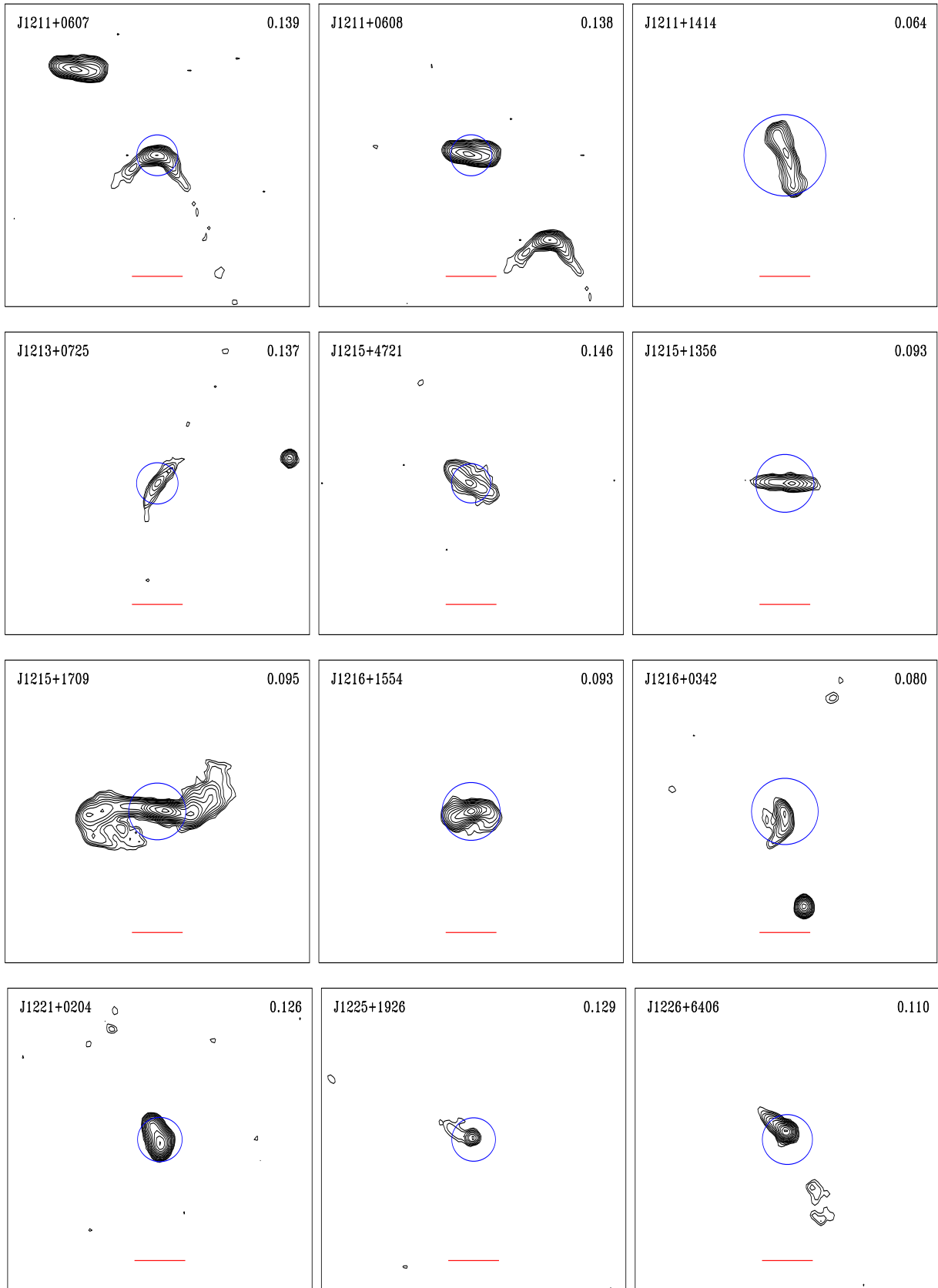


Fig. A.1. continued.

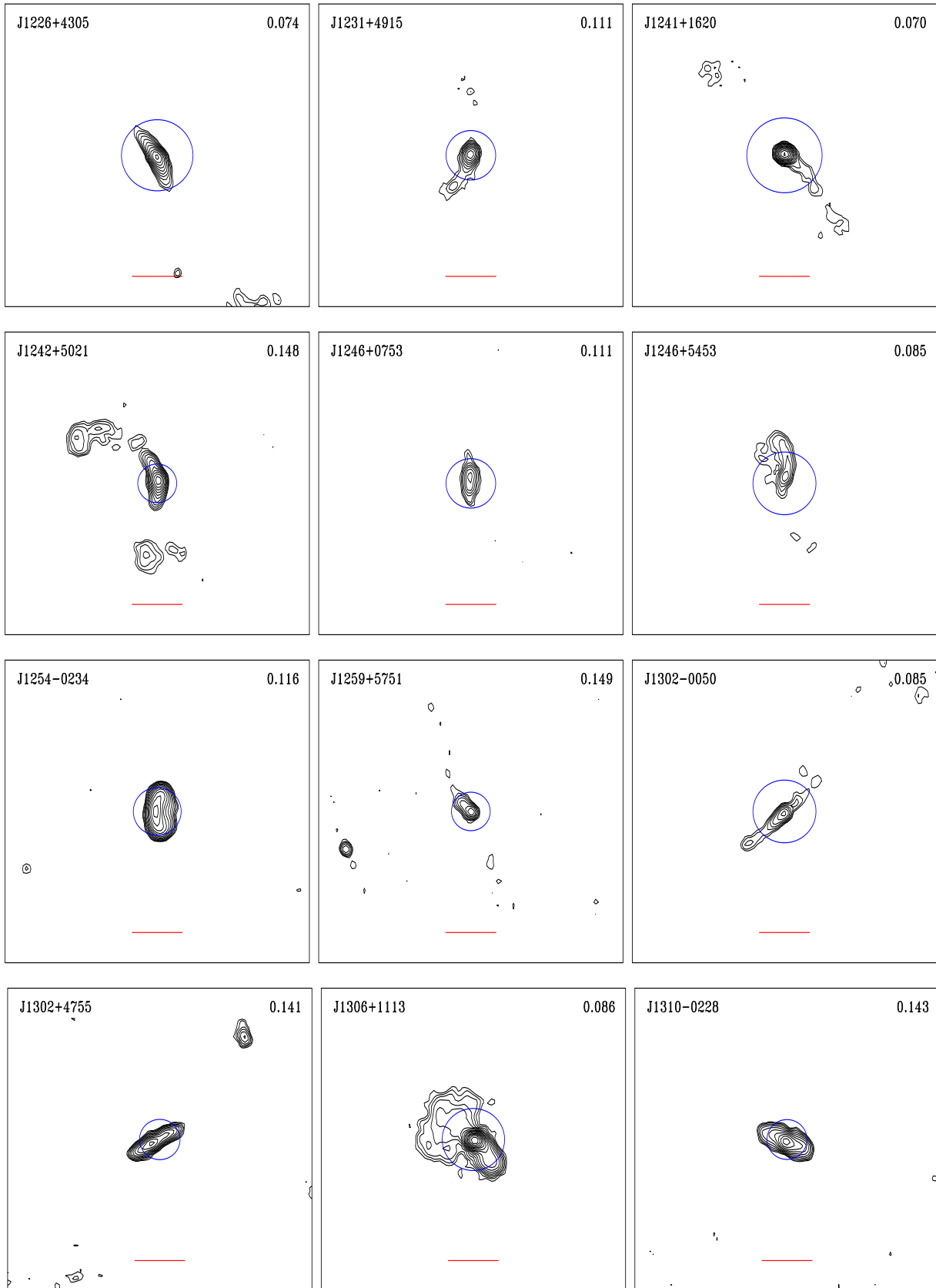


Fig. A.1. continued.

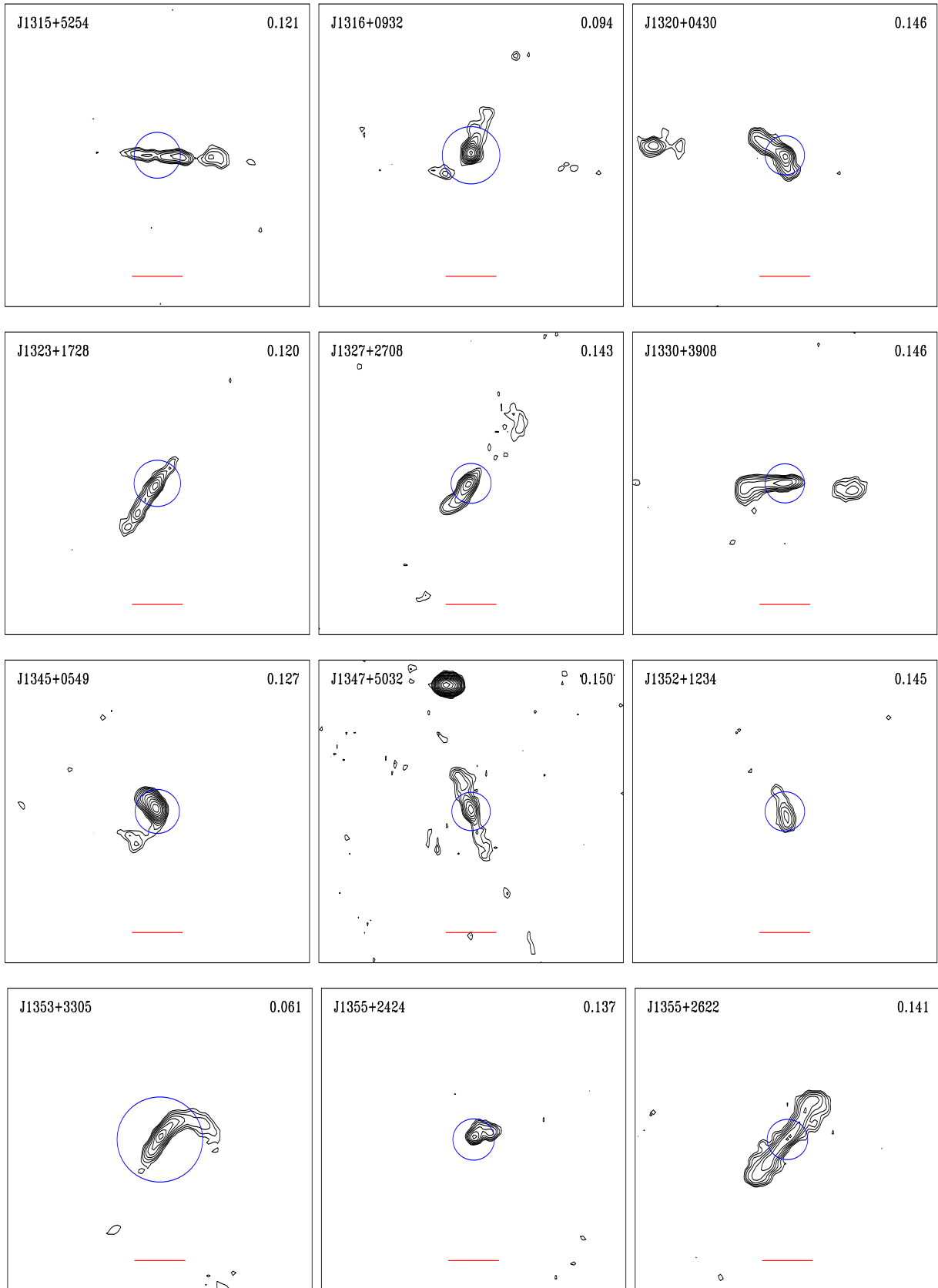


Fig. A.1. continued.

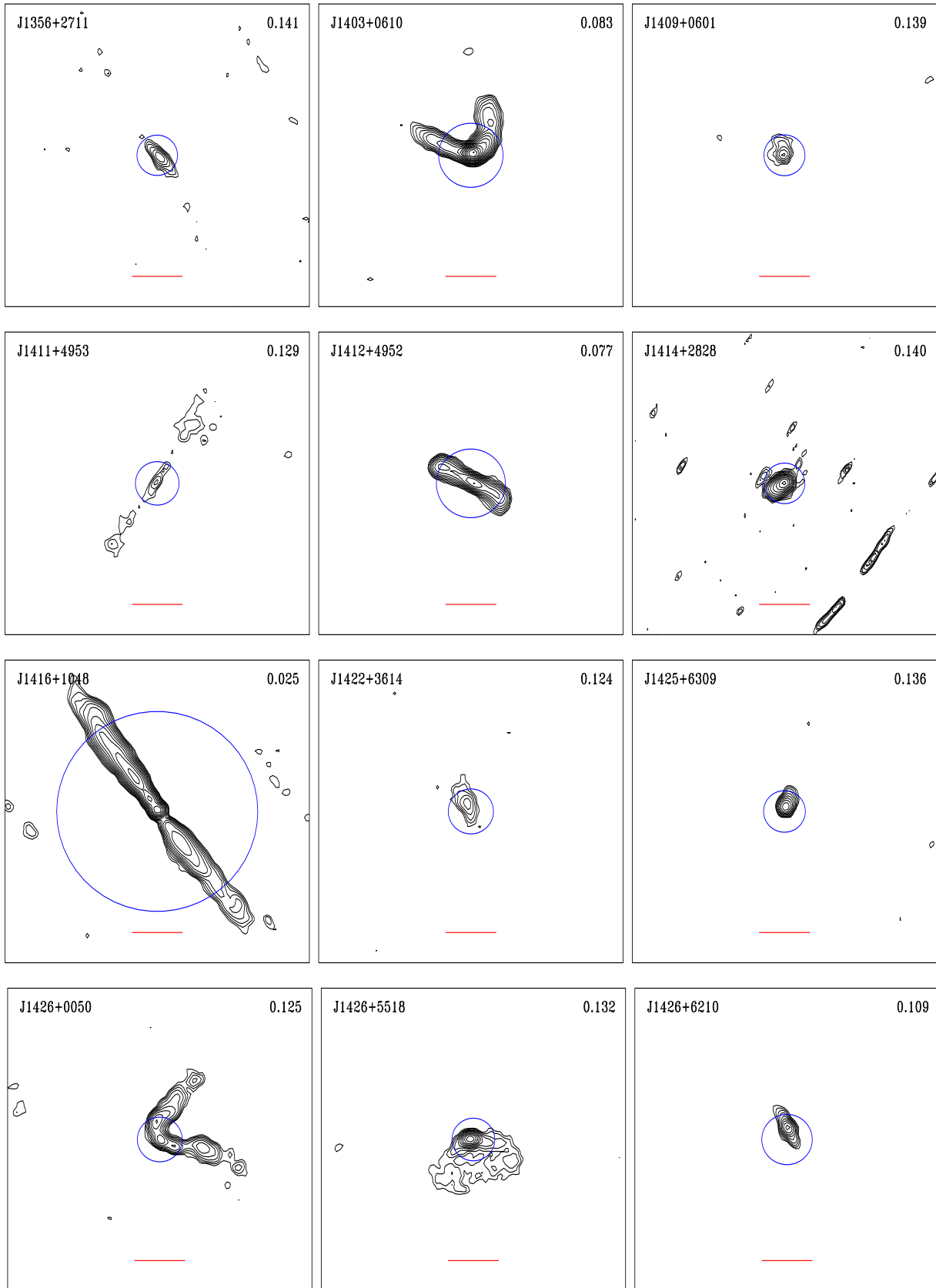


Fig. A.1. continued.

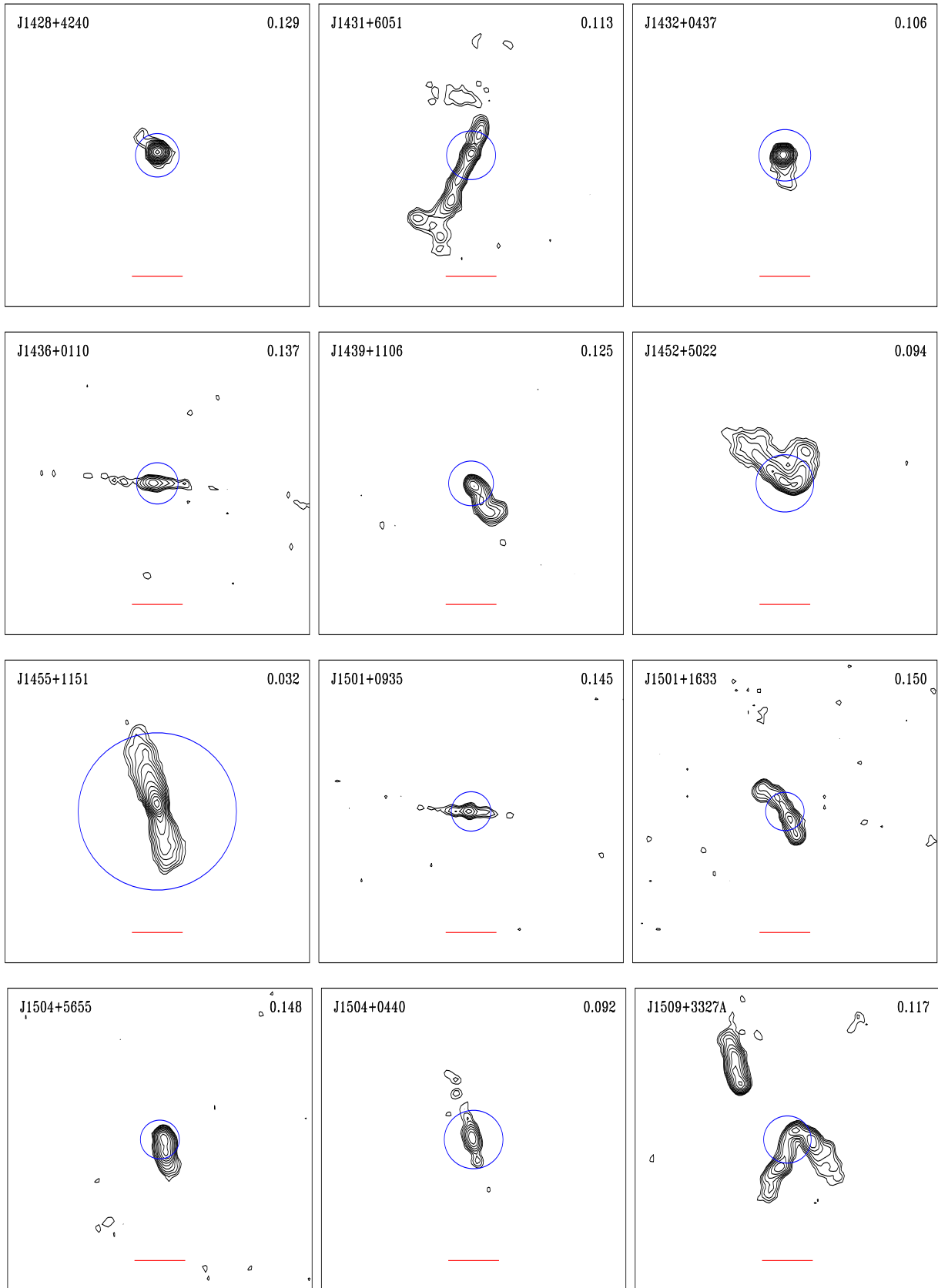


Fig. A.1. continued.

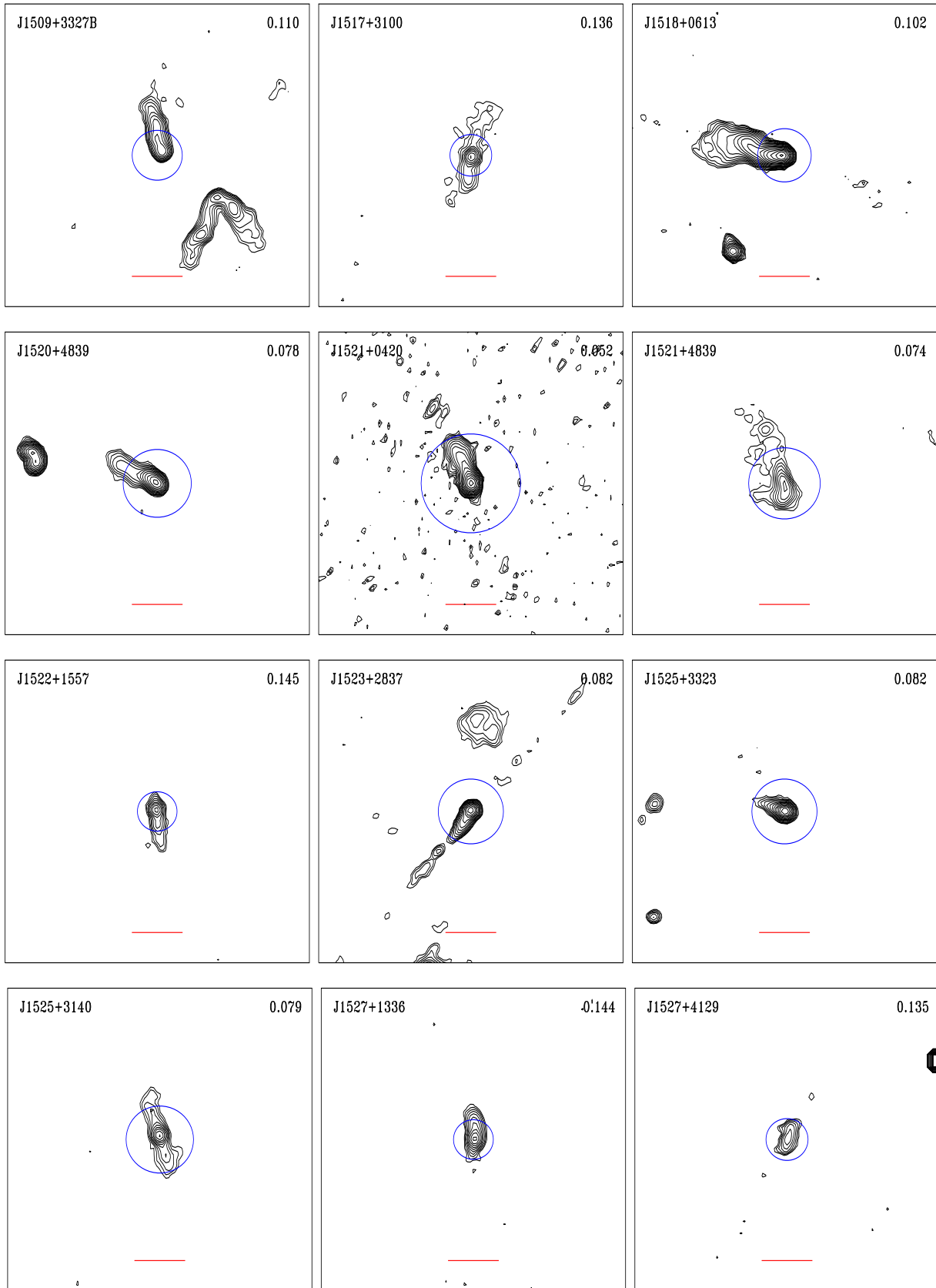


Fig. A.1. continued.

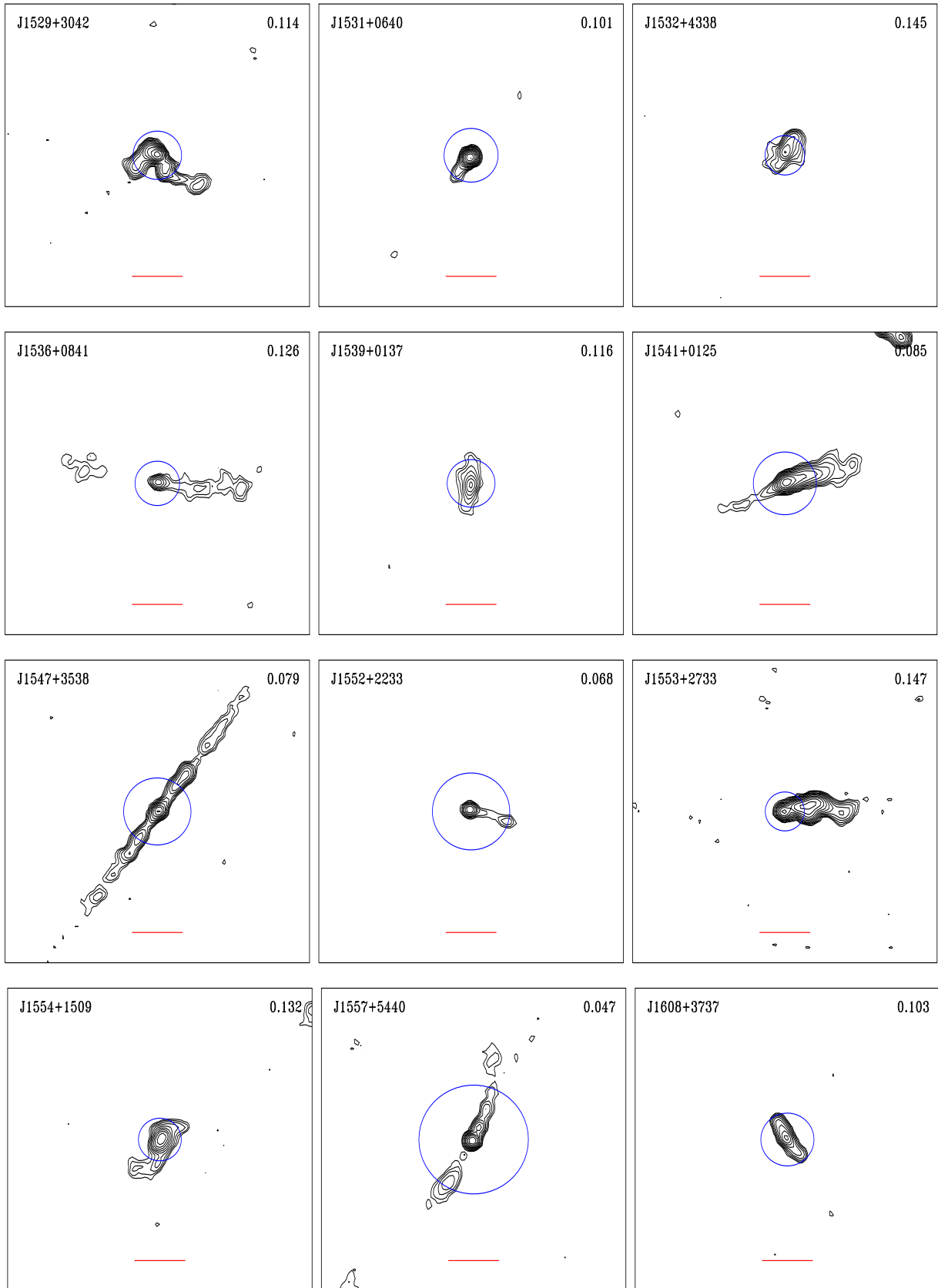


Fig. A.1. continued.

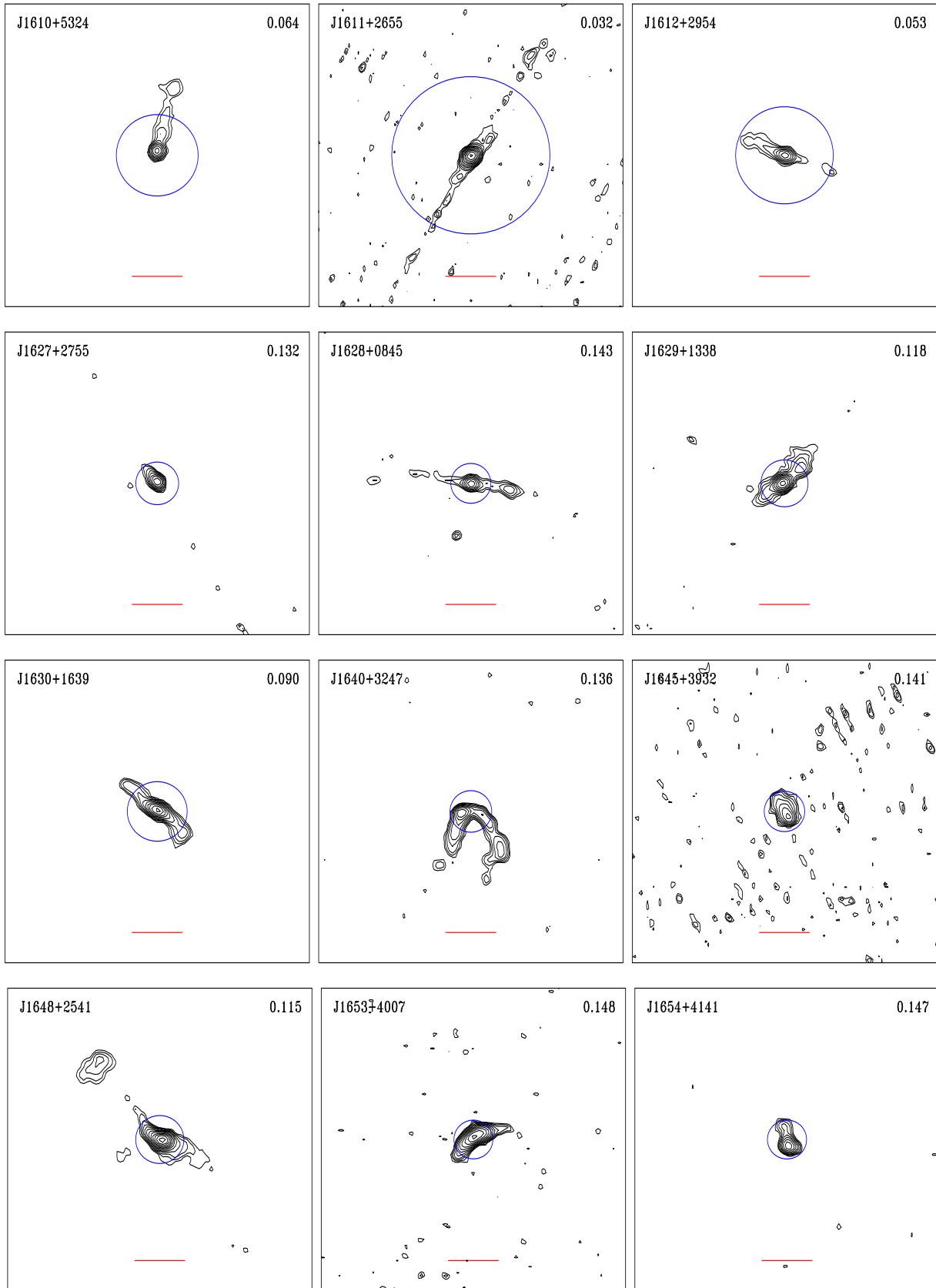


Fig. A.1. continued.

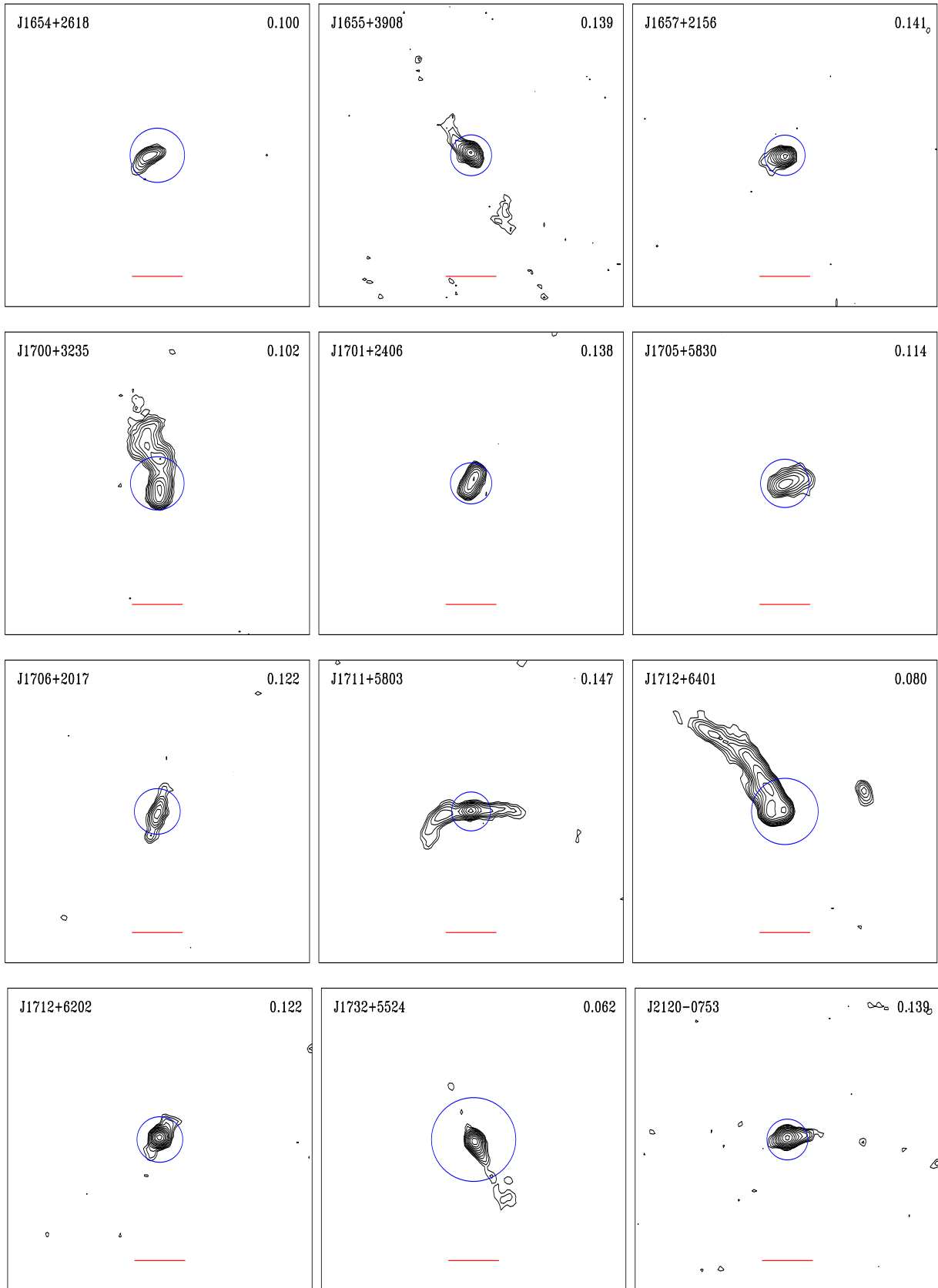


Fig. A.1. continued.

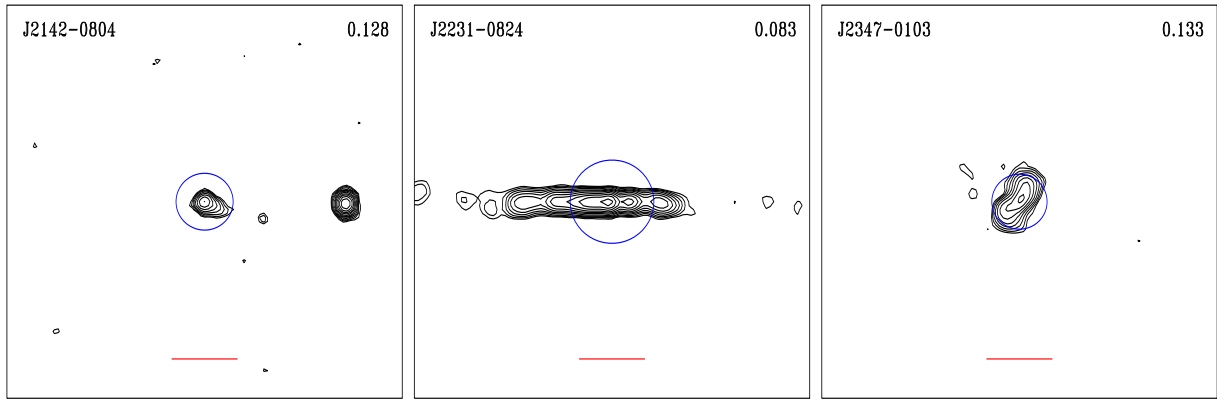


Fig. A.1. continued.

## Appendix B: Additional tables

Table B.1. Properties of the FRICAT sources.

	$z$	NVSS	[O III]	$m_r$	Dn	$\sigma_*$	$C_r$	$\nu L_r$	$L_{[\text{O III}]}$	$M_{\text{BH}}$
SDSS J002900.98-011341.7	0.083	282.8	158.5	14.637	1.76	321	3.33	40.86	40.46	9.0
SDSS J003930.52-103218.6	0.129	23.7	1.9	15.996	1.97	238	3.14	40.19	38.94	8.4
SDSS J004148.22-091703.1	0.053	53.0	25.6	15.230	2.01	255	3.01	39.72	39.26	8.6
SDSS J004300.63-091346.3	0.076	148.4	40.7	15.437	1.96	244	3.32	40.50	39.79	8.5
SDSS J004530.46-004746.9	0.147	12.4	15.1	16.266	2.02	287	3.08	40.03	39.97	8.8
SDSS J011255.11-095040.6	0.124	81.7	20.8	16.026	1.84	220	2.99	40.69	39.95	8.3
SDSS J013327.25-082416.4	0.149	218.8	31.9	16.076	2.01	331	3.35	41.29	40.31	9.0
SDSS J013412.78-010729.4	0.079	119.6	39.6	15.152	2.03	262	3.55	40.44	39.81	8.6
SDSS J013503.43-005427.6	0.080	39.3	27.8	14.628	2.00	300	3.25	39.96	39.67	8.8
SDSS J014029.59+001825.8	0.148	12.3	8.2	16.642	1.95	278	3.34	40.03	39.71	8.7
SDSS J015253.79-001005.5	0.082	13.1	22.8	16.487	2.01	187	3.43	39.52	39.61	8.0
SDSS J025227.52-075605.4	0.078	99.7	10.4	15.348	1.95	237	3.00	40.35	39.22	8.4
SDSS J025437.99+005621.9	0.067	116.0	52.4	14.903	1.99	272	3.18	40.27	39.78	8.7
SDSS J073014.37+393200.4	0.142	11.3	5.3	16.716	2.07	223	3.08	39.96	39.48	8.3
SDSS J073505.25+415827.5	0.087	67.6	21.9	17.308	1.95	256	2.29	40.28	39.65	8.6
SDSS J073719.18+292932.0	0.111	43.0	4.7	16.038	2.03	231	2.84	40.30	39.19	8.4
SDSS J074125.85+480914.3	0.120	25.7	13.0	16.540	1.94	230	2.91	40.16	39.72	8.4
SDSS J074351.25+282128.0	0.106	20.2	15.5	16.206	1.94	252	3.34	39.94	39.68	8.5
SDSS J075309.91+355557.1	0.113	94.6	9.0	16.304	1.85	246	2.98	40.67	39.50	8.5
SDSS J075506.67+262115.9	0.123	46.0	3.1	16.483	1.94	265	3.03	40.43	39.12	8.6
SDSS J080113.28+344030.8	0.083	45.0	5.5	15.641	2.03	226	3.13	40.06	39.00	8.3
SDSS J080326.62+303725.0	0.144	7.4	1.0	15.829	1.98	301	2.97	39.79	38.75	8.8
SDSS J080923.10+211546.2	0.142	10.6	11.8	16.910	1.88	255	3.09	39.93	39.83	8.6
SDSS J081523.21+115715.1	0.100	40.0	3.6	15.468	1.85	251	3.27	40.18	39.00	8.5
SDSS J081604.40+112449.4	0.122	34.6	14.9	16.156	1.96	281	3.43	40.30	39.79	8.7
SDSS J081614.27+425657.6	0.127	121.0	11.3	16.628	1.98	240	3.09	40.88	39.70	8.4
SDSS J081849.74+040631.5	0.095	61.5	18.3	15.841	1.85	233	3.18	40.32	39.64	8.4
SDSS J081932.66+200748.8	0.117	31.8	11.5	16.888	1.79	222	3.17	40.23	39.64	8.3
SDSS J082025.14+160123.2	0.148	44.2	19.3	17.505	2.00	225	2.92	40.59	40.08	8.3
SDSS J082028.09+485347.3	0.132	188.1	12.3	15.666	2.01	295	2.72	41.11	39.78	8.8
SDSS J082603.81+471910.3	0.128	25.7	2.3	16.288	1.98	231	3.49	40.22	39.02	8.4
SDSS J082729.73+530733.4	0.119	22.9	16.7	16.942	1.88	184	2.93	40.10	39.81	8.0
SDSS J082733.62+160053.7	0.091	53.0	12.2	15.474	1.96	250	3.20	40.21	39.43	8.5
SDSS J082926.46+224436.3	0.087	148.8	9.3	15.623	2.00	223	3.19	40.62	39.27	8.3
SDSS J083138.83+223422.9	0.087	185.3	39.4	15.441	1.89	302	3.32	40.72	39.90	8.8
SDSS J083159.69+303930.7	0.107	20.9	52.4	15.572	1.99	246	3.18	39.96	40.21	8.5
SDSS J083224.13+164949.1	0.102	20.2	23.6	15.896	1.92	304	3.37	39.90	39.83	8.9
SDSS J084140.57+254827.9	0.140	29.1	10.6	16.353	1.97	241	3.30	40.35	39.77	8.5
SDSS J084159.65+500551.7	0.141	7.6	3.8	16.677	2.06	259	3.15	39.78	39.33	8.6
SDSS J085321.54+331629.9	0.126	28.1	15.7	15.838	1.92	266	2.93	40.24	39.84	8.6
SDSS J085719.46+241142.6	0.133	11.8	10.9	16.694	2.06	220	3.20	39.92	39.73	8.3
SDSS J090018.16+074535.5	0.061	70.6	31.0	14.308	1.88	261	3.20	39.97	39.46	8.6
SDSS J090245.43+164710.4	0.130	15.2	7.9	16.049	2.02	243	3.16	40.00	39.57	8.5
SDSS J090543.54+401704.8	0.128	46.0	9.7	15.924	1.89	277	3.29	40.47	39.65	8.7
SDSS J091442.02+152155.7	0.140	28.3	7.0	16.839	1.86	235	3.32	40.35	39.60	8.4
SDSS J092049.04+403952.8	0.074	21.9	17.2	15.980	2.04	258	3.40	39.64	39.39	8.6
SDSS J092935.02+625659.3	0.121	50.9	19.4	15.785	1.90	281	3.11	40.46	39.89	8.7
SDSS J093058.74+034827.7	0.089	111.0	22.9	15.135	2.01	276	3.16	40.51	39.68	8.7
SDSS J093305.27+291015.1	0.132	53.6	12.3	15.743	1.97	254	3.34	40.56	39.78	8.5

**Notes.** Column description: (1) source name; (2) redshift; (3) NVSS 1.4 GHz flux density [mJy]; (4) [O III] flux [in  $10^{-17}$  erg  $\text{cm}^{-2}$   $\text{s}^{-1}$  units]; (5) SDSS DR7  $r$  band  $AB$  magnitude; (6) concentration index  $C_r$ ; (7) Dn(4000) index; (8) stellar velocity dispersion [ $\text{km s}^{-1}$ ]; (9) logarithm of the radio luminosity [ $\text{erg s}^{-1}$ ]; (10) logarithm of the [O III] line luminosity [ $\text{erg s}^{-1}$ ]; (11) logarithm of the black hole mass [in solar units].

Table B.1. continued.

	$z$	NVSS	[O III]	$m_r$	Dn	$\sigma_*$	$C_r$	$\nu L_r$	$L_{[\text{O III}]}$	$M_{\text{BH}}$
SDSS J094202.04+105818.3	0.136	14.4	3.5	16.613	1.90	242	3.28	40.02	39.26	8.5
SDSS J094332.99+334158.3	0.131	23.9	2.8	15.974	1.91	276	3.24	40.21	39.14	8.7
SDSS J094614.50+581937.6	0.147	80.9	21.7	15.995	1.97	307	3.14	40.85	40.13	8.9
SDSS J095527.76+034516.8	0.091	47.0	–	16.615	1.81	190	3.10	40.16	–	8.0
SDSS J100451.83+543404.3	0.047	121.8	56.9	13.980	1.95	269	3.38	39.98	39.50	8.6
SDSS J100757.06+280147.9	0.148	27.3	11.5	15.864	1.99	309	3.26	40.38	39.86	8.9
SDSS J100804.13+502642.8	0.134	53.7	1.9	16.736	2.00	218	3.23	40.58	38.98	8.3
SDSS J101114.38+191425.7	0.149	31.5	11.8	16.531	1.89	269	3.38	40.45	39.87	8.6
SDSS J101545.46+311500.2	0.125	15.6	4.4	16.869	1.77	211	3.09	39.98	39.28	8.2
SDSS J101937.94+001955.7	0.096	43.0	31.7	15.251	1.96	275	3.16	40.17	39.89	8.7
SDSS J102008.61+174817.4	0.122	19.5	0.7	16.405	1.92	240	3.46	40.05	38.43	8.4
SDSS J102314.24+483122.0	0.148	31.1	17.0	16.331	1.98	296	3.24	40.44	40.03	8.8
SDSS J102603.83+390524.0	0.145	108.1	11.0	17.009	1.89	258	2.84	40.96	39.82	8.6
SDSS J102703.83+382013.0	0.123	41.0	9.0	15.916	1.87	209	3.17	40.38	39.58	8.2
SDSS J103036.15+355459.8	0.124	50.0	8.5	15.487	2.05	325	3.40	40.47	39.56	9.0
SDSS J103126.60+115250.5	0.144	25.2	12.7	16.291	1.98	259	3.15	40.32	39.87	8.6
SDSS J103258.88+564453.2	0.045	213.4	114.6	13.549	1.97	280	3.08	40.18	39.76	8.7
SDSS J103827.01+414852.9	0.125	43.0	14.7	16.366	1.82	193	3.23	40.42	39.80	8.1
SDSS J103930.43+394718.9	0.093	23.3	15.6	15.075	1.96	274	3.34	39.88	39.56	8.7
SDSS J104045.34+395448.5	0.134	35.8	2.5	16.888	1.91	235	2.98	40.40	39.11	8.4
SDSS J104049.99+561508.1	0.134	22.3	15.9	16.123	1.77	257	3.25	40.20	39.90	8.6
SDSS J104233.38+363946.5	0.142	53.1	2.0	16.347	1.82	243	2.95	40.63	39.06	8.5
SDSS J104855.28+311945.2	0.117	52.2	10.4	15.607	1.93	270	3.08	40.44	39.59	8.7
SDSS J104907.26+551314.9	0.126	24.0	23.8	15.440	1.89	448	3.30	40.17	40.02	9.5
SDSS J104921.13–004005.0	0.039	250.0	70.2	13.544	1.90	226	2.83	40.11	39.42	8.3
SDSS J105147.39+552308.3	0.074	522.0	48.5	14.624	2.08	320	3.54	41.02	39.84	9.0
SDSS J105259.97+430255.0	0.148	52.0	23.6	16.414	1.87	225	3.32	40.66	40.17	8.3
SDSS J105344.12+492955.9	0.140	64.3	33.4	16.012	1.30	262	3.49	40.70	40.27	8.6
SDSS J105348.93+402345.9	0.128	100.1	1.2	15.592	1.97	283	3.22	40.81	38.72	8.7
SDSS J105544.98+452401.4	0.064	133.5	6.8	14.706	2.02	213	3.34	40.29	38.85	8.2
SDSS J105702.79+564503.1	0.136	15.4	4.1	16.207	2.02	304	3.39	40.05	39.33	8.9
SDSS J105847.67+164526.0	0.116	49.4	16.4	16.261	1.88	226	3.35	40.41	39.79	8.3
SDSS J110535.78+091956.3	0.127	22.3	6.1	16.110	2.00	251	3.23	40.15	39.44	8.5
SDSS J111020.07+204657.5	0.135	12.9	2.9	16.509	1.97	275	3.38	39.97	39.18	8.7
SDSS J111037.33+541135.7	0.141	23.5	15.7	16.449	1.99	206	3.08	40.27	39.95	8.2
SDSS J111211.37+304352.3	0.106	43.5	24.5	15.990	1.95	244	3.29	40.27	39.87	8.5
SDSS J111337.13+234846.5	0.140	8.4	17.4	16.842	1.96	249	3.33	39.82	39.99	8.5
SDSS J111911.13+081539.8	0.076	80.0	25.6	15.054	2.05	257	3.16	40.22	39.58	8.6
SDSS J112055.83+173854.0	0.085	21.5	9.4	15.623	1.97	205	2.85	39.75	39.25	8.2
SDSS J112352.34+443735.6	0.139	22.9	10.1	17.434	1.90	273	3.85	40.24	39.74	8.7
SDSS J112403.19+475814.9	0.140	28.2	3.0	16.675	1.97	266	3.22	40.35	39.22	8.6
SDSS J112457.40+171744.7	0.142	9.5	5.0	16.147	2.00	285	3.03	39.88	39.46	8.8
SDSS J112603.59+545329.1	0.149	16.0	12.4	16.871	1.94	258	3.46	40.16	39.90	8.6
SDSS J113012.79+235822.1	0.140	46.5	19.8	16.474	1.80	265	3.60	40.56	40.05	8.6
SDSS J113359.23+490343.4	0.032	732.0	84.7	13.126	1.90	264	3.30	40.40	39.32	8.6
SDSS J114210.72+552729.6	0.133	24.9	8.8	16.099	2.01	218	3.05	40.24	39.64	8.3
SDSS J114212.11+101159.0	0.103	46.6	9.1	16.086	1.89	243	3.10	40.28	39.42	8.5
SDSS J114345.53+192333.4	0.094	37.8	17.0	15.411	2.00	237	3.17	40.10	39.61	8.4
SDSS J115109.39+435918.6	0.071	75.0	37.5	14.982	1.92	216	3.17	40.13	39.69	8.3
SDSS J115323.89+305904.8	0.136	43.2	8.9	16.911	1.97	191	3.30	40.50	39.67	8.1
SDSS J115508.97+232623.4	0.144	26.4	12.6	17.279	2.00	245	2.98	40.34	39.87	8.5
SDSS J115729.60+292308.1	0.140	16.6	9.3	17.195	2.01	224	3.32	40.11	39.71	8.3
SDSS J115816.37+340605.9	0.131	19.8	26.3	16.311	1.85	221	3.16	40.13	40.11	8.3
SDSS J115936.05+233947.5	0.142	31.8	5.0	16.510	1.92	282	3.51	40.41	39.45	8.7

Table B.1. continued.

	$z$	NVSS	[O III]	$m_r$	Dn	$\sigma_*$	$C_r$	$\nu L_r$	$L_{[\text{O III}]}$	$M_{\text{BH}}$
SDSS J120021.93–020152.7	0.146	40.4	24.8	16.336	2.04	248	3.12	40.54	40.18	8.5
SDSS J120401.47+201356.3	0.024	402.1	111.6	12.997	1.81	270	3.25	39.91	39.21	8.7
SDSS J120425.29+034510.6	0.149	54.7	4.2	16.608	1.95	248	3.14	40.69	39.43	8.5
SDSS J120522.29+050941.4	0.136	105.0	0.6	16.002	2.02	335	3.47	40.88	38.49	9.0
SDSS J120943.62–020459.6	0.100	32.3	23.3	15.922	1.98	253	3.34	40.09	39.80	8.5
SDSS J121110.99+060744.1	0.139	50.9	12.8	16.154	1.94	221	3.12	40.59	39.84	8.3
SDSS J121114.07+060833.9	0.138	78.5	11.1	16.143	1.96	238	3.18	40.78	39.78	8.4
SDSS J121121.12+141439.2	0.064	62.0	56.4	14.783	2.03	233	3.13	39.96	39.77	8.4
SDSS J121332.93+072516.9	0.137	17.2	10.9	15.739	1.92	242	3.00	40.11	39.76	8.5
SDSS J121519.19+472142.4	0.146	31.1	2.9	17.108	0.00	193	3.09	40.42	39.25	8.1
SDSS J121534.18+135635.0	0.093	30.9	21.1	15.362	2.04	303	3.15	40.00	39.69	8.9
SDSS J121543.82+170917.6	0.095	460.0	40.0	14.538	1.99	312	2.86	41.19	39.99	8.9
SDSS J121619.95+155417.7	0.093	77.2	19.0	15.228	1.81	210	3.11	40.40	39.64	8.2
SDSS J121640.12+034231.5	0.080	207.0	24.0	15.677	1.99	243	3.22	40.69	39.61	8.5
SDSS J122156.16+020450.8	0.126	119.5	9.5	16.885	1.92	232	3.40	40.87	39.62	8.4
SDSS J122532.09+192615.2	0.129	25.6	23.9	17.363	1.82	192	3.05	40.22	40.05	8.1
SDSS J122622.49+640622.0	0.110	81.0	43.6	15.516	1.82	257	3.09	40.58	40.16	8.6
SDSS J122640.83+430509.2	0.074	33.5	18.4	14.836	1.98	272	3.15	39.83	39.42	8.7
SDSS J123128.93+491537.0	0.111	52.1	5.1	16.192	1.85	217	3.06	40.39	39.24	8.3
SDSS J124135.94+162033.6	0.070	165.0	77.2	15.040	1.95	305	3.31	40.47	39.99	8.9
SDSS J124207.38+502146.6	0.148	102.0	14.3	16.365	1.97	237	3.33	40.95	39.95	8.4
SDSS J124622.48+075327.9	0.111	19.8	23.4	15.774	1.95	275	3.25	39.97	39.89	8.7
SDSS J124647.52+545315.0	0.085	38.5	32.6	14.974	2.01	268	3.09	40.01	39.79	8.6
SDSS J125434.93–023412.4	0.116	122.6	2.0	15.959	1.93	260	3.30	40.80	38.86	8.6
SDSS J125953.32+575149.7	0.149	15.5	5.5	17.347	1.71	211	3.17	40.14	39.55	8.2
SDSS J130203.58–005012.3	0.085	73.7	30.2	14.964	2.10	243	3.27	40.29	39.76	8.5
SDSS J130248.70+475510.6	0.141	47.9	20.0	15.563	1.95	301	3.06	40.58	40.05	8.8
SDSS J130619.24+111339.7	0.086	321.0	44.5	14.926	1.72	267	3.04	40.94	39.94	8.6
SDSS J131053.44–022841.5	0.143	53.0	12.7	16.792	2.04	267	2.77	40.64	39.87	8.6
SDSS J131531.07+525437.3	0.121	37.1	0.5	16.470	2.01	247	3.31	40.33	38.30	8.5
SDSS J131613.54+093236.7	0.094	42.0	23.6	15.558	1.95	293	3.43	40.14	39.74	8.8
SDSS J132017.54+043037.4	0.146	30.5	4.4	15.935	1.81	229	2.59	40.42	39.42	8.4
SDSS J132302.49+172832.9	0.120	38.7	13.9	16.128	1.92	242	3.36	40.34	39.75	8.5
SDSS J132736.13+270816.8	0.143	34.2	11.2	16.081	2.03	267	3.35	40.45	39.82	8.6
SDSS J133038.01+390815.4	0.146	47.5	14.3	16.858	1.93	236	3.22	40.61	39.94	8.4
SDSS J134529.50+054952.9	0.127	54.2	15.8	16.498	1.97	240	3.21	40.53	39.85	8.4
SDSS J134745.19+503203.5	0.150	18.2	1.3	16.204	2.06	244	3.35	40.21	38.91	8.5
SDSS J135214.56+123401.7	0.145	11.0	–	16.729	2.02	239	3.44	39.96	–	8.4
SDSS J135302.04+330528.5	0.061	80.0	22.1	14.703	1.93	208	3.24	40.03	39.32	8.2
SDSS J135511.34+242415.6	0.137	16.1	4.1	16.713	1.90	270	3.08	40.08	39.34	8.7
SDSS J135553.63+262217.9	0.141	69.8	6.9	15.904	1.94	294	3.17	40.74	39.59	8.8
SDSS J135655.28+271120.2	0.141	16.3	13.5	16.061	1.93	253	3.06	40.11	39.88	8.5
SDSS J140313.28+061008.2	0.083	256.6	76.9	15.097	1.87	340	3.23	40.81	40.14	9.1
SDSS J140916.74+060139.4	0.139	10.8	25.3	16.844	1.91	218	3.37	39.92	40.14	8.3
SDSS J141138.22+495304.0	0.129	27.5	16.5	16.478	2.12	230	3.10	40.25	39.88	8.4
SDSS J141243.83+495206.5	0.077	101.4	24.0	14.643	2.04	303	3.23	40.35	39.58	8.9
SDSS J141427.10+282830.5	0.140	77.1	9.4	16.420	1.72	263	3.30	40.78	39.72	8.6
SDSS J141652.94+104826.7	0.025	4581.1	228.7	12.057	1.97	341	3.06	40.98	39.53	9.1
SDSS J142206.79+361434.8	0.124	13.7	17.5	16.742	1.73	226	2.75	39.91	39.87	8.3
SDSS J142521.22+630921.3	0.136	19.8	7.7	15.833	1.89	273	3.22	40.16	39.60	8.7
SDSS J142616.34+005015.3	0.125	88.7	10.1	15.878	1.97	254	2.98	40.73	39.64	8.6
SDSS J142623.76+551804.9	0.132	52.8	8.5	16.254	1.96	205	3.30	40.56	39.62	8.2
SDSS J142649.23+621005.9	0.109	25.9	28.5	15.539	1.94	306	3.40	40.07	39.97	8.9
SDSS J142832.60+424021.0	0.129	56.4	48.0	16.182	1.18	251	3.23	40.57	40.35	8.5

Table B.1. continued.

	$z$	NVSS	[O III]	$m_r$	Dn	$\sigma_*$	$C_r$	$\nu L_r$	$L_{[\text{O III}]}$	$M_{\text{BH}}$
SDSS J143147.54+605109.4	0.113	163.0	27.7	15.726	1.94	251	3.19	40.90	39.99	8.5
SDSS J143257.81+043715.1	0.106	68.6	21.8	15.767	1.99	302	3.14	40.46	39.82	8.9
SDSS J143638.56+011058.8	0.137	19.2	15.9	15.944	2.02	326	2.98	40.16	39.93	9.0
SDSS J143928.78+110613.8	0.125	39.8	12.7	16.068	1.67	247	2.86	40.39	39.74	8.5
SDSS J145215.46+502225.1	0.094	133.8	13.9	15.124	1.99	246	3.14	40.65	39.52	8.5
SDSS J145555.27+115141.4	0.032	382.0	142.0	13.224	1.98	287	3.30	40.12	39.54	8.8
SDSS J150111.50+093547.9	0.145	15.2	15.3	16.549	1.98	246	3.09	40.10	39.96	8.5
SDSS J150148.14+163345.6	0.150	37.2	3.9	16.488	1.98	225	3.36	40.53	39.40	8.3
SDSS J150408.01+565545.4	0.148	57.3	12.4	16.708	1.98	276	3.30	40.70	39.89	8.7
SDSS J150450.51+044054.8	0.092	53.6	7.7	15.848	1.89	227	2.99	40.23	39.24	8.3
SDSS J150957.37+332715.0	0.117	66.0	11.7	15.956	1.97	266	3.24	40.54	39.65	8.6
SDSS J150959.74+332746.1	0.110	66.0	25.0	16.560	1.90	232	3.10	40.49	39.92	8.4
SDSS J151744.96+310015.8	0.136	49.0	7.1	16.224	1.94	291	3.21	40.55	39.57	8.8
SDSS J151845.72+061356.1	0.102	487.0	26.0	15.589	1.31	297	3.63	41.28	39.86	8.8
SDSS J152045.04+483922.9	0.078	80.6	19.8	15.917	2.12	257	3.04	40.26	39.50	8.6
SDSS J152122.54+042030.1	0.052	452.0	51.4	13.936	1.85	280	2.93	40.64	39.55	8.7
SDSS J152126.99+483943.2	0.074	63.3	17.4	15.628	2.10	256	3.14	40.10	39.40	8.6
SDSS J152235.19+155707.6	0.145	25.2	15.2	16.575	2.11	298	3.28	40.33	39.96	8.8
SDSS J152326.91+283732.5	0.082	733.0	48.9	15.021	1.93	234	3.16	41.26	39.94	8.4
SDSS J152500.83+332359.8	0.082	75.5	52.6	15.232	1.84	243	3.21	40.27	39.96	8.5
SDSS J152522.33+314037.1	0.079	51.4	33.7	15.541	2.01	250	3.35	40.07	39.74	8.5
SDSS J152715.31+133650.9	0.144	47.2	25.9	16.172	2.00	291	2.88	40.59	40.19	8.8
SDSS J152737.36+412947.1	0.135	14.3	–	16.562	2.00	222	3.07	40.02	–	8.3
SDSS J152945.60+304235.6	0.114	88.0	27.8	15.252	2.05	356	3.55	40.64	40.00	9.1
SDSS J153138.76+064045.5	0.101	40.1	47.2	14.959	1.83	312	3.25	40.19	40.12	8.9
SDSS J153215.31+433844.5	0.145	26.8	15.9	16.593	1.96	250	3.17	40.35	39.98	8.5
SDSS J153621.11+084112.1	0.126	68.1	18.6	16.255	2.00	266	3.31	40.63	39.92	8.6
SDSS J153932.09+013710.5	0.116	20.1	26.6	16.279	1.99	278	2.93	40.02	39.99	8.7
SDSS J154155.16+012517.4	0.085	113.0	24.5	15.291	1.96	276	3.25	40.48	39.67	8.7
SDSS J154709.22+353846.1	0.079	213.9	36.2	14.574	2.06	355	3.01	40.70	39.78	9.1
SDSS J155222.36+223311.9	0.068	44.8	40.0	14.802	2.04	267	3.44	39.88	39.68	8.6
SDSS J155311.93+273320.6	0.147	115.0	9.0	15.829	1.98	271	2.89	41.00	39.75	8.7
SDSS J155401.99+150946.8	0.132	50.5	19.7	16.590	1.99	240	3.21	40.54	39.98	8.5
SDSS J155721.38+544015.9	0.047	90.0	91.8	13.930	1.79	289	3.44	39.84	39.71	8.8
SDSS J160816.32+373743.1	0.103	40.4	13.3	16.018	1.99	248	3.30	40.21	39.59	8.5
SDSS J161037.77+532421.0	0.064	61.2	48.6	14.847	2.02	287	3.43	39.95	39.71	8.8
SDSS J161114.11+265524.2	0.032	102.8	111.1	13.437	1.97	263	3.42	39.56	39.44	8.6
SDSS J161242.69+295404.7	0.053	36.1	5.6	14.666	1.98	215	3.29	39.56	38.61	8.3
SDSS J162700.42+275547.7	0.132	14.5	8.7	16.157	1.96	264	2.97	40.00	39.63	8.6
SDSS J162806.20+084538.0	0.143	35.8	8.3	16.376	1.97	279	3.46	40.47	39.69	8.7
SDSS J162918.66+133824.0	0.118	72.0	15.6	16.093	1.96	249	3.31	40.59	39.78	8.5
SDSS J163043.14+163910.8	0.090	52.0	7.4	15.700	2.03	224	3.39	40.19	39.20	8.3
SDSS J164053.90+324728.4	0.136	50.0	5.4	16.458	1.97	226	3.19	40.56	39.45	8.3
SDSS J164548.45+393227.4	0.141	25.4	37.4	17.304	1.75	186	3.02	40.30	40.33	8.0
SDSS J164845.08+254119.5	0.115	102.6	8.8	16.201	2.02	228	3.13	40.72	39.50	8.4
SDSS J165304.98+400702.5	0.148	87.7	19.4	16.423	1.96	256	3.27	40.89	40.09	8.6
SDSS J165425.53+414121.2	0.147	17.2	6.8	17.283	1.91	201	3.04	40.17	39.62	8.1
SDSS J165448.44+261841.3	0.100	18.8	44.1	15.677	1.97	256	3.31	39.86	40.08	8.6
SDSS J165500.19+390847.9	0.139	54.8	17.5	15.887	2.05	358	3.42	40.63	39.99	9.1
SDSS J165744.77+215611.1	0.141	25.5	23.2	16.862	1.86	277	3.49	40.30	40.12	8.7
SDSS J170011.22+323514.7	0.102	185.0	9.1	15.734	1.87	239	3.26	40.86	39.41	8.4
SDSS J170115.59+240608.4	0.138	26.0	5.2	17.079	2.08	240	3.26	40.30	39.46	8.4
SDSS J170543.99+583001.2	0.114	26.9	–	16.436	1.97	183	3.20	40.13	–	8.0
SDSS J170602.20+201757.8	0.122	29.3	5.1	15.824	1.93	295	3.16	40.23	39.32	8.8

**Table B.1.** continued.

	$z$	NVSS	[O III]	$m_r$	Dn	$\sigma_*$	$C_r$	$\nu L_r$	$L_{[\text{O III}]}$	$M_{\text{BH}}$
SDSS J171137.98+580330.2	0.147	42.0	18.6	16.354	2.11	312	3.32	40.56	40.06	8.9
SDSS J171223.15+640157.1	0.080	150.0	10.8	15.848	2.02	235	3.03	40.55	39.26	8.4
SDSS J171243.95+620245.0	0.122	47.2	19.4	16.243	1.86	274	3.35	40.43	39.90	8.7
SDSS J173223.73+552452.8	0.062	54.8	42.6	15.093	2.09	247	3.24	39.88	39.62	8.5
SDSS J212005.00-075350.1	0.139	48.2	22.4	16.844	2.02	263	3.21	40.57	40.09	8.6
SDSS J214239.29-080423.8	0.128	13.9	8.9	16.904	1.95	231	3.19	39.95	39.61	8.4
SDSS J223143.19-082431.7	0.083	766.0	61.1	14.149	2.01	301	2.86	41.29	40.04	8.8
SDSS J234702.42-010300.9	0.133	34.3	5.8	17.507	1.83	202	2.98	40.38	39.46	8.1

**Table B.2.** Properties of the sFRICAT sources.

	$z$	NVSS	[O III]	$m_r$	Dn	$\sigma_*$	$C_r$	$\nu L_r$	$L_{[\text{O III}]}$	$M_{\text{BH}}$
SDSS J090100.09+103701.7	0.029	63.3	162.2	13.254	1.96	250	3.46	39.27	39.54	8.5
SDSS J092122.11+545153.9	0.045	36.6	50.5	14.217	1.95	253	3.35	39.41	39.40	8.5
SDSS J092151.48+332406.5	0.024	117.3	109.4	13.127	1.95	227	3.34	39.34	39.17	8.4
SDSS J093957.34+164712.8	0.047	41.3	49.3	14.982	1.70	217	2.95	39.51	39.44	8.3
SDSS J101623.01+601405.6	0.031	35.0	58.1	13.244	1.95	251	3.24	39.07	39.15	8.5
SDSS J104740.48+385553.6	0.035	55.9	49.9	13.255	1.96	304	3.36	39.39	39.19	8.9
SDSS J111125.21+265748.9	0.034	86.8	87.5	13.322	1.99	281	2.91	39.53	39.38	8.7
SDSS J132451.44+362242.7	0.017	789.4	394.5	12.662	2.01	242	3.32	39.91	39.46	8.5
SDSS J133242.54+071938.1	0.023	152.5	169.9	12.987	1.81	237	2.86	39.45	39.35	8.4
SDSS J145222.83+170717.8	0.045	102.8	20.4	14.226	1.94	240	3.05	39.86	39.01	8.4
SDSS J155603.90+242652.9	0.043	127.0	91.9	14.064	1.86	252	3.12	39.90	39.62	8.5
SDSS J155749.61+161836.6	0.037	113.4	70.4	13.100	2.00	328	2.99	39.73	39.38	9.0
SDSS J160332.08+171155.2	0.034	662.0	79.0	13.549	2.02	298	3.45	40.42	39.35	8.8
SDSS J160722.95+135316.4	0.034	75.1	46.3	13.554	1.99	268	3.41	39.47	39.11	8.6

**Notes.** Column description: (1) source name; (2) redshift; (3) NVSS 1.4 GHz flux density [mJy]; (4) [O III] flux [in  $10^{-17}$  erg cm $^{-2}$  s $^{-1}$  units]; (5) SDSS DR7  $r$  band  $AB$  magnitude; (6) concentration index  $C_r$ ; (7) Dn(4000) index; (8) stellar velocity dispersion [km s $^{-1}$ ]; (9) logarithm of the radio luminosity [erg s $^{-1}$ ]; (10) logarithm of the [O III] line luminosity [erg s $^{-1}$ ]; (11) logarithm of the black hole mass [in solar units].